PPPL-2156

DR-0656-4
I-18431

PPPL-2156

UC20-F

CHARGE-EXCHANGE MEASUREMENTS OF BEAM ION THERMALIZATION IN MHD-QUIESCENT PLASMAS IN THE POLOIDAL DIVERTOR EXPERIMENT

By

R. Kaita et al.

OCTOBER 1984

PLASMA PHYSICS LABORATORY

PRINCETON UNIVERSITY
PRINCETON, NEW JERSEY

PREPARED FOR THE U.S. DEPARTMENT OF ENERGY,
UNDER CONTRACT DE-AC02-76-CHO-3073.

CHARGE-EXCHANGE MEASUREMENTS OF BEAM ION THERMALIZATION IN MHD-QUIESCENT PLASMAS IN THE POLOIDAL DIVERTOR EXPERIMENT

PPPL--2156

DE85 004167

R. Kaita, R.J. Goldston, P. Beiersdorfer, D.L. Herndon, S.M. Kaye, H.W. Kugel, R.T. McCann, D.C. McCune, D.D. Meyerhofer, and H.H. Towner

ABSTRACT

The horizontally scanning, multiangle charge-exchange analyzer on the Poloidal Divertor Experiment (PDX) was used to study the beam ion slowing-down process with high-power perpendicular injection. Measurements were made over a wide range in toroidal field (8 kG < B(T) < 22 kG), plasma current (200 kA < I(p) < 500 kA), and beam power (1 MW < P_B < 7 MW). In MHD-quiescent plasmas, good agreement is found between the measured slowing-down spectra and theoretical predictions as a function of both angle and energy. Classes of prompt orbit losses are observed with both co- and counter-injection which have been understood and applied to plasma diagnostics. The effects of MHD activity on fast ion thermalization will be the subject of a companion paper.

I. INTRODUCTION

Auxiliary heating of tokamaks with neutral beams[1] has proved to be successful in achieving high plasma temperatures and values of β_T in many experiments during the last decade. Tangential injection into low density, highly collisionless plasmas was used to obtain the highest temperatures in tokamaks to date,[2] and recently, injection perpendicular to the magnetic axis[3] has been studied in experiments to maximize beta at higher plasma densities.

One facility particularly suited for such studies is the Poloidal Divertor Experiment (PDX) at the Princeton Plasma Physics Laboratory, which is equipped with four near-perpendicular neutral heating beams oriented for co-injection (Fig. 1). The beams were designed and constructed at the Oak Ridge National Laboratory (ORNL), and are capable of injecting 7.2 MW of deuterium beams or 5.5 MW of hydrogen beams using four 50-keV ion sources.[4] Typical pulse durations are from 150 to 350 msec.

On PDX, we have the unique capability of obtaining slowing-down spectra during neutral beam heating experiments through the use of a horizontally scanning neutral particle analyzer[5] with fast time response. Its position relative to the heating beams is shown in Fig. 1, and the five closely spaced sightlines emanating from the analyzer correspond to its five viewing angles when it is in its most perpendicular position.

Fast neutrals from charge exchange along these sightlines are energy-analyzed by electrostatic deflection plates. The 127-degree curved cylindrical plates are connected to two high voltage operational amplifiers, which in turn are typically driven by a 10 Hz triangular waveform generator. Thus, a complete energy spectrum is obtained every 50 msec by ramping the plate voltage. The particle detectors themselves are multianode microchannel plates operated in current mode, and because of their fast time response, the

thickness of the analyzer's stripping cell, and the close location of the analyzer to the plasma, the analyzer's ability to study transient phenomena is limited primarily by the 10-μsec response of the signal amplifiers.

The fast time resolution was more important in the study of high β_T discharges in PDX,[6] where it was necessary to measure the 10- to 20-kHz internal structure of "fishbone" bursts. Since the focus of the present work is on MHD-quiescent discharges, the effects of these phenomena on the beam ion thermalization process will not be discussed here. Instead, the emphasis will be on the extensive measurements of slowing-down spectra obtained during the systematic variation of the toroidal field, plasma current, and neutral beam power during deuterium injection into hydrogen limiter plasmas. Results from H-mode divertor and scoop limiter plasmas will also be presented.

Bounce-averaged Fokker-Planck calculations[7] gave reasonable agreement with the data from the high toroidal field and plasma current discharges, as did Monte-Carlo beam orbit calculations,[8] which also predicted the correct magnitude as well as the shape of the slowing-down spectra. However, recycling at the "standard" and scoop limiter positions served as toroidally local neutral sources which had to be modelled to simulate the data obtained during these discharges.

II. EXPERIMENTAL SLOWING-DOWN SPECTRA

A. Toroidal field, plasma current, and beam power scans

Slowing-down spectra were obtained during deuterium injection into deuterium and hydrogen plasmas at high toroidal fields and plasma currents. The results shown in Fig. 2 are for a 22-kG toroidal field and a deuterium plasma current of 380 kA. The five curves correspond to the flux measured along the sightlines illustrated in Fig. 1. The analyzer is oriented for

detecting counter-moving ions, so for co-injection on PDX, only the trapped ions that charge exchange on the inside "leg" of banana orbits can be observed. The most perpendicular sightline views these ions directly, that is, even along collisionless trajectories. The flux measured at this angle is depicted by the uppermost curve in Fig. 2.

Deuterium injection in hydrogen limiter plasmas was studied under a variety of toroidal fields, plasma currents, and neutral beam powers. The present discussion will be restricted to data from 12-kG and 15-kG discharges, since plasmas at lower toroidal fields, and hence higher values of $\beta_T q$, were no longer MHD quiescent. The plasma conditions corresponding to the many slowing-down spectra comprising Figs. 3 and 4 are listed in Tables I and II. In the absence of significant MHD activity, the magnitude of the measured fast neutral flux appears to scale linearly with beam power. As T_e rises with injection, the relative signal in the off-angle channels increases as expected. At higher beam powers and lower toroidal fields, "fishbone" oscillations[6] are observed on the slowing-down spectra. The energy "peaks" measured by the FIDE analyzer are a spurious effect of the sweeping detection voltage, coupled with repetitive MHD bursts. The average flux of beam ions with energies between the injection energy and half the injection energy, measured along the most perpendicular analyzer sightline, is plotted as a function of the absorbed beam power in Figs. 5a and 5b. Aside from a few cases where the fishbone instability has a clear effect on the beam ion distribution (the 400 kA, 12 kG cases), there is a linear dependence of the flux with beam power.

The Princeton transport analysis code TRANSP, [8-11] which will be described in more detail in Sec. IIIB, was used to simulate the slowing-down spectra shown in Figs. 3 and 4. An estimate of the particle confinement time

was obtained in each case by adjusting its value (or equivalently, the neutral density profile) in TRANSP until the absolute magnitude of the experimental and calculated particle fluxes agreed. The results are plotted in Figs. 5c and 5d. Although there is considerable scatter, the general trend appears to indicate an improvement in confinement time with increasing plasma current.

As was the case with the 12 kG slowing-down spectra shown in Fig. 4, a significant exception occurs at the highest current and beam powers due to the onset of the fishbone instability. Such effects will be discussed in a companion publication,[12] and the 400-kA, 12-kG plasma confinement times are not plotted in Fig. 5d, due to the problematic validity of this kind of analysis for them.

B. High confinement regime

Recent results from the ASDEX group[13] concerning a high confinement (H-mode) regime in divertor plasmas prompted systematic and detailed investigations of such discharges in PDX. Figure 6 shows the time variation of the charge-exchange efflux at 35 keV along the most perpendicular sightline of the analyzer. At the transition to the H-mode, the signal drops by a factor of 1.3 to 2.0 at essentially all energies and angles which correspond to the beam thermalization signal. This is consistent with a significant improvement in the particle confinement time, since at the same time that this result indicates a fall in the neutral density (n_0), a substantial dn/dt begins. In this regime, there are also periodic spikes in the charge-exchange signal, which are correlated with bursts in the hydrogen Lyman-alpha emission. These are quite different from the fishbone spikes observed during high $\beta_T q$ experiments.[6] Typically, the spikes are about 1-msec long, and constitute a factor of two enhancement in the charge-exchange signal. They

are observed about equally, in relative magnitude, at all angles and energies corresponding to the beam thermalization signal. Thus, the simplest explanation is that the neutral density doubles during this time, perhaps due to the recycling of plasma particles lost due to an instability. This topic will be treated in more detail in a subsequent publication.[12]

III. COMPARISONS WITH MODEL CALCULATIONS

A. Bounce-averaged Fokker-Planck calculations

Under conditions of high toroidal fields and plasma currents (low $\beta_T q$), the relatively small banana orbits allow us to use a bounce-averaged Fokker-Planck calculation to simulate the data.[7] The finite banana width was taken into account for beam ion deposition and detection by computing the mapping of the orbit between the injection or detection point and the known banana tip. In the Fokker-Planck calculation, fast ions are assumed to be located at the minor radius of their banana tips.

One neutral heating beam parameter to which the slowing-down spectra are sensitive is the percentage of each species component. There is typically a full, one-half, and one-third energy species, the latter two corresponding to the dissociation of H_2^+ (D_2^+) and H_3^+ (D_3^+) accelerated by the beam system. These manifest themselves as discontinuities in the slowing-down spectra at each energy (Fig. 2), and their magnitudes are proportional to the fraction of the beam in each component.

Recently, the beam species fractions have been determined directly by looking at the particle yields from the Rutherford backscattering of the beam off the titanium carbide PDX inner wall armor, in the absence of a plasma.[14] The same particle analyzer was used in this measurement, and since this is an in situ technique, it has the advantage of determining the beam fractions

actually entering the tokamak, instead of test stand values, which may be different. Analysis of these data is still underway, but preliminary results (Fig. 7) show that the particle fractions at the full, one-half, and one-third energies varied from 0.33, 0.37, and 0.30 to 0.55, 0.30, and 0.15 as the analyzer scanned across the inner wall armor. An average species mix of 0.45:0.30:0.25 was used in the simulation codes, and it gives good agreement with the slowing-down spectra. The predicted differences in the flux between adjoining channels, however, are somewhat less than what they were experimentally (Fig. 2). Agreement with the data did improve with the better treatment of finite banana width effects in the Monte-Carlo simulation calculations, which are discussed in the next section.

B. Monte-Carlo simulation calculations

Slowing-down spectra were also calculated using a Monte-Carlo simulation algorithm in TRANSP. This treatment allowed us to improve the modelling finite-banana width effects, thus obtaining more accurate values for the fast neutral flux detected by the FIDE analyzer for lower current plasmas. The beam ion slowing-down process is governed by small angle binary collisions as described by a Fokker-Planck operator of the form discussed in Ref. 8.

To perform the simulation, we first require a spatially two-dimensional beam distribution function, and Fig. 8 shows the spatial zones used in TRANSP.[15] Energy is used as one velocity space dimension, since it gives good resolution from thermal energies to above the beam injection energy, typically 50 keV. The pitch-angle dimension is parametrized by $v_{\parallel}/v$, which is a convenient variable because the FIDE analyzer is sensitive to particles with

$$v_{\parallel}/v = R_{tan}/R_{view}, \tag{1}$$

where R_{tan} is the analyzer tangency radius (Fig. 1), and R_{view} is the spatial location along a given sightline which is being viewed. Since R_{tan} is generally incremented in roughly even steps in the experimental measurements, even spacing in $v_{\parallel}/v$ is appropriate to give a matching angular resolution in the calculation.

The beam distribution function is accumulated by first tracking particles along trajectories determined by the known ion source geometry. Deposition is calculated using a Monte-Carlo simulation for exponential attenuation,[8] and the beam ion orbits are followed in discrete time steps. At each interval, the particle's position in the beam distribution coordinate system is determined, and the value of the distribution in the appropriate bin is incremented. A constant census of 1000 Monte-Carlo particles are followed in the time dependent calculation, and a time span of 50 msec is typically averaged for calculating the fast neutral flux.

The technique used to obtain the fast neutral flux along a given analyzer sightline is shown schematically in Fig. 9. Tracking along the chord is done in small, even increments and the length of sightline within each spatial and pitch-angle zone is evaluated by interpolation. The total simulated flux is accumulated by adding up the signal from each sightline element. The result of this process can then be compared with the actual measurement along the given analyzer sightline.

Predictions for the "zero banana width limit," where the toroidal field and plasma current were set to be effectively infinite in the TRANSP and bounce-averaged Fokker-Plank codes, are shown in Fig. 10. The two codes do not entirely agree for sightlines closest to the tangency radius of the

heating beams (i.e., the most perpendicular sightlines, which have the highest flux levels in Fig. 10), because they do not treat beam divergence in the same way.[15] However, both codes predict the same spread in the flux between the most perpendicular and most parallel analyzer sightlines in this high toroidal field, high plasma current limit. Figure 11 shows the experimental and TRANSP slowing-down spectra for conditions similar to those in Fig. 2 and again, the computed results follow the trend of the data. However, there is now a tendency to overestimate the spread between adjoining channels, a problem that will be dealt with below.

Figure 12 shows a slowing-down spectrum obtained with two deuterium beams in a deuterium divertor plasma. Since we did not have to model any unusual effects like the loss mechanism present during fishbones, we could perform a straightforward comparison between the absolute magnitudes as well as the shapes of the experimental and calculated slowing-down spectra. The agreement with the interchannel spread and the absolute magnitude in Fig. 12 suggests that we do have a fairly good understanding of the beam ion thermalization process from the evidence provided by charge-exchange measurements.

Slowing-down spectra were also obtained during scoop limiter discharges (Fig. 13). With both the bounce-averaged Fokker-Planck calculations and the Monte-Carlo approach, it was difficult to reproduce spread in the measured neutral flux between adjacent sightlines. Increased pitch-angle scattering due to a high Z_{eff} would result in more flux along more parallel sightlines, and this was simulated in both types of calculations. However, the concomitant beam ion loss below the injection energy was not seen experimentally in these limiter discharges, and since there was no evidence from other measurements to suggest a high Z_{eff}, this was not considered a likely explanation.

The analyzer was fairly close (38 degrees in toroidal angle) to the scoop limiters, which act as an additional nonaxisymmetric neutral source not present in divertor discharges. Therefore, the resulting enhancement of the central neutral density would mean that the limiter-enhanced flux along each sightline came proportionately more from the center than the edge of the plasma. There would thus be less variation from channel to channel than expected if the charge-exchange flux were dominated by neutrals generated from the walls of the vacuum vessel as assumed in the model originally in our calculations.

Figure 13 compares the calculated spectra using the TRANSP Monte-Carlo model with results from scoop limiter plasmas. The good agreement in the most perpendicular channel in absolute magnitude is consistent with a long (180 msec) particle confinement time. Even with the limiter as a source of neutrals close to the analyzer, the absolute magnitude of the flux is much lower than in the divertor case (Fig. 12). However, the TRANSP code only includes a toroidally averaged wall source of neutrals, and the difference in the flux between adjoining sightlines is not predicted very well.

A three-dimensional Monte-Carlo beam neutrals code, NBDEN,[16] was used to generate a more realistic neutral density distribution. The scoop limiter was simulated by a point source at the outer wall in the horizontal midplane of the vacuum vessel. The results were then used as input for the bounce-averaged Fokker-Planck program cited earlier.[7] The TRANSP calculation was also repeated with only a toroidally averaged volume source of neutrals to simulate roughly the contribution of the scoop limiter. The spectra generated by the two codes are comparable (Fig. 14). This suggests that the scoop may indeed cause a local enhancement in the central neutral density as seen by the neutral particle analyzer 38° away from it. The spectrum calculated with this

improved model is compared with the data in Fig. 15, and there is better agreement with the relative flux between adjacent channels.

A similar analysis was performed to simulate slowing-down spectra obtained during H-mode divertor plasmas. Instead of a point source, plasma fuelling with gas from the upper dome was duplicated by a toroidal line source located above the plasma center at the outer wall in NBDEN. This had the effect of increasing the central neutral density, and as in the scoop limiter case, caused the bounce-averaged Fokker-Planck program to predict a smaller variation from analyzer sightline to sightline than when a wall neutral source alone was used. The results from a TRANSP calculation with H-mode plasma parameters, but only a toroidally averaged volume neutral source, are compared with the data in Fig. 16.

III. OTHER RESULTS AND CONCLUSIONS

A. Counter-injection and potential measurements

Counter-injection with four deuterium beams into a hydrogen limiter plasma was also studied. The injection angles are unchanged but now, the deposition of the beam neutrals occurs on the inside "leg" of the banana orbits.[17] Particles detected by the analyzer must thus charge exchange on the outside leg of the banana orbit, along a more parallel sightline. In Fig. 17, the uppermost curve now corresponds to the flux along the most parallel analyzer sightline, and the Monte-Carlo calculations correctly predict this change in viewing geometry from the new orbit topology.

Although the toroidal field was fairly low (8.4 kG), there is no evidence in the slowing-down spectra of the MHD activity seen during co-injection under similar plasma conditions.[6] Also, the peaking at the full, half, and third energies corresponds to "prompt" losses of beam ions as they

pass in front of the analyzer on their first toroidal transit, and charge-exchange in the region of high neutral density near the edge. Such peaks are not as conspicuous during co-injection, but are still present.

To confirm this interpretation, single co-injecting neutral beams were injected into successive discharges. As expected, the East beamline (when co-injecting) had the most conspicuous peaks (Fig. 18). The relative heights of the full energy peaks were then plotted (Fig. 19) to determine the exponential decrease in their size as a function of toroidal distance from the analyzer. From Fig. 18, the height of the peak (Δf_D) drops by 1/e after a toroidal distance (Δ_ϕ) of 1.5 radians. If τ_ϕ is the time needed to travel Δ_ϕ,

$$\tau_\phi = \frac{\Delta_\phi R_0}{v_\phi} \tag{2}$$

where

$$v_\phi \simeq \frac{v_\parallel^2 + v_\perp^2/2}{\Omega_0 R_0} \cdot \frac{B_\phi}{B_\theta} \ . \tag{3}$$

R_0 is the major radius, Ω_0 is the gyrofrequency, and B_ϕ and B_θ are the toroidal and poloidal magnetic fields, respectively. For 45 keV ions in PDX, $\tau_\phi = 4.9 \times 10^{-6}$ sec. This time is also related to the edge neutral density (n_0) and the charge-exchange cross section (σv) by

$$\tau_\phi = \frac{1}{n_0 \sigma v} \ . \tag{4}$$

Using the value of σv from Ref. 18, we obtain $n_0 = 1.7 \times 10^{12}$ cm^{-3}. This prompt loss peak has a width in excess of the detector's bandwidth of $\Delta E/E \cong 3\%$. This may be due to dispersion in slowing-down rates. The beam slowing-down time, τ_s, is

$$\tau_s = \frac{6.32 \times 10^8 \, A_b}{Z_b^2 \, \ell n \, \Lambda_e} \cdot \frac{T_e^{3/2}}{n_e} \qquad (5)$$

where A_b and Z_b are the atomic weight and number, respectively, of the neutral beam species, and $\ln\Lambda_e$ is obtained from Hinton and Hazeltine.[19] But

$$\frac{\tau_\phi}{\tau_s} = \frac{\Delta v}{v} = \frac{\Delta E}{2E} \qquad (6)$$

where E = 45 keV (the injection energy), and ΔE is the energy (2 keV) the beam ions transfer to the bulk plasma in the time τ_ϕ, as estimated from the spread of the prompt peak in Fig. 17. This means that $\tau_s = 2.2 \times 10^{-4}$ sec.

Solving for $n_e/T_e^{3/2}$,

$$\frac{n_e}{T_e^{3/2}} = \frac{6.32 \times 10^8 \, A_b}{Z_b^2 \, \ell n \, \Lambda_e} \cdot \frac{1}{2.2 \times 10^{-4} \text{sec}} = 5.4 \times 10^{11} \text{ cm}^{-3} \text{ eV}^{-3/2}. \qquad (7)$$

This is consistent with an electron density of $n_e = 8 \times 10^{12}$ cm^{-3}, and $T_e = 6$ eV.

B. Potential measurements

By carefully examining beam ion orbits during counter-injection, it is possible to deduce information about the current profile and plasma potentials. The calculated first half-orbits for counter-injected ions are shown in Fig. 20. We expect both passing and banana orbits to be confined, and particles captured in the outer region of the plasma are lost on large bananas. For plasma currents in the 350 kA range, there is a small class of

loss orbits between the confined banana and passing orbits. These originate from the center of the tokamak, and their presence or absence is a fairly sensitive measurement of q(0). For a counter-injection scoop plasma, $q(0) \gtrsim 1.4$ for these orbits to be seen.

Consistent with this picture, narrow peaks are indeed seen near the injection energy in two distinct angular ranges during counter injection in moderate current (350 kA) scoop limiter plasmas. Figure 21a shows the normal edge loss peak, while Fig. 21c shows the new central loss peak at a much more tangential angle. Between these two ranges, the slowing-down spectrum is normal (Fig. 21b). The amplitude of the loss peak is plotted as a function of analyzer aiming major radius in Fig. 22. Because the orbits move outward in major radius as they turn from counter to co, the $v_\perp/v$ at which they are detected is lower than that with which they were injected. Therefore, the tangency radius for the banana loss orbits in the outer region is somewhat greater than the neutral beam injector tangency radius of 35-cm. However, we also observe the second strong peak at a much more parallel angle. If μ-conservation is assumed, these particles had to be originally ionized deep in the plasma if they were counter-injected at a 35 cm tangency radius. The calculations used to determine the trajectories shown in Fig. 20 predict a tangency radius for detecting these central loss orbits which is very close to the measured value.

The prompt peaks in Figs. 21a and 21c are also shifted in energy relative to each other. For the scoop plasma studied, the central loss orbits were shifted by about 600 eV relative to the edge loss orbits. Reconstructing the orbits for these particular angles, the birth radii appear to be 8 and 18 cm for the "central" and "normal edge" loss orbits. The energy shift suggests a space potential difference of about 600 eV between 8 and 18 cm, giving a

rotation speed of 5 to 10 × 10^7 cm/sec using $v_\phi = cE_r/B_p$, consistent with other measurements.[20] Additional measurements as a function of radial position were made using a horizontally scanning collimated diagnostic neutral beam,[21] injected tangentially. In this case, one looks at the energy of the peak of the slowing-down spectrum on each side of the injected orbits, inboard and outboard of the magnetic axis. Energy shifts of the peak of the spectrum were then interpreted as a potential difference transversed due to the orbit shift $\Delta r = 2qv_\parallel/\Omega_{ci}$. Rotation speeds in the range of 3 x 10^6 cm/sec were deduced near the edge of the plasma, again consistent with other measurements.[20]

C. CONCLUSIONS

Slowing-down spectra were measured over a wide range of toroidal fields, plasma currents, and beam powers. Modelling of toroidally local neutral sources was required to provide good agreement between the experimental data and theoretical calculations, particularly in limiter discharges. In MHD-quiescent plasmas, the charge-exchange flux scaled linearly with beam power. The slowing-down spectra were classical in these plasmas, and absolute determinations of the charge-exchange flux provided a measure of the neutral density. We thus had a means of estimating the particle confinement time, which appeared to improve with plasma current.

Finite banana width corrections also had to be included to simulate a number of effects. The peaking of the charge-exchange flux along parallel sightlines far from the near-perpendicular injection angle of the neutral beams suggested the existence of central loss orbits with large effective banana widths. The "prompt" charge-exchange loss peak near the beam injection energies also seemed to indicate radial excursions of beam ions into the

region of high neutral density beyond the plasma periphery. Estimates of edge parameters were also deduced from this effect, and they were consistent with results from other diagnostics.

ACKNOWLEDGMENTS

The authors wish to express their gratitude toward the PDX group, whose skillful collaboration and emphasis on systematic scans of plasma parameters made this study possible. We give special thanks to K. Bol, M. Bell, M. Okabayashi, D.K. Owens, and H. Takahashi for their responsibilities in PDX machine operations; R. Budny, R. Fonck, B. Grek, D. Johnson, B. LeBlanc, K. McGuire, and G. Schmidt for the many plasma diagnostics necessary for the understanding of these experiments; and H. Eubank, M. Williams, and the injection group for the highly reliable performance of the PDX neutral beam system. This work was supported by U. S. Department of Energy Contract DE-AC02-76-CHO-3073.

REFERENCES

[1]T. H. Stix, Plasma Phys. 14, 367 (1972).

[2]H. P. Eubank et al., in Proc. of the 7th Int. Conf. on Plasma Physics and Controlled Nucl. Fus. Res., (Innsbruck, 1978).

[3]TFR Group, (to be published).

[4]W. L. Gardner et al., in Proc. of the 8th Int. Conf. on Plasma Phys. and Controlled Nucl. Fus. Res., (Brussels, 1980), Vol. II, 547 (1981).

[5]R. Kaita, R. J. Goldston, D. D. Meyerhofer, and J. Eridon, Rev. Sci. Instrum. 52, 1975 (1981).

[6]K. McGuire et al., Phys. Rev. Lett. 50, 891 (1983).

[7]J. G. Cordey, Nucl. Fusion 16, 499 (1976).

[8]R. J. Goldston, D. C. McCune, H. H. Towner, S. L. Davis, R. J. Hawryluk, and G. L. Schmidt, J. Comput. Phys. 43, 61 (1981).

[9]R. J. Hawryluk, "An Empirical Approach to Tokamak Transport," in Course on Physics of Plasmas Close to Thermonuclear Conditions, Varenna, Italy, 1979.

[10]D.C. McCune, R.C. Hawryluk, R.T. McCann, G.L. Schmidt, Bull. Am. Phys. Soc. 27, 971 (1982).

[11]R.T. McCann, R.J. Goldston, D.C. McCune, Bull. Am. Phys. Soc. 27, 971 (1982).

[12]R. J. Goldston et al., to be published.

[13]F. Wagner et al., Phys. Rev. Lett. 49, 1408 (1982).

[14]H. W. Kugel et al., Bull. Am. Phys. Soc. 27, 1049 (1982).

[15]R.T. McCann, R.J. Goldston, S.M. Kaye, D.C. McCune, Bull. Am. Phys. Soc. 28, 1222 (1983).

[16]H. H. Towner and R. J. Goldston, Bull. Am. Phys. Soc. 24, 1107 (1979).

[17]J. A. Rome and Y.-K. M. Peng, Nucl. Fusion 19, 9 (1979).

[18]S. K. Allison and M. Garcia-Munoz, "Electron Capture and Loss at High Energies," in Atomic and Molecular Processes, edited by D. R. Bates (Academic, New York, 1962).

[19]F. L. Hinton and R. D. Hazeltine, Rev. Mod. Phys. 48, 239 (1976).

[20]K. Brau, M. Bitter, R.J. Goldston, D. Manos, K. McGuire, and S. Suckewer, Nucl. Fusion 23, 1643 (1983).

[21]A. Nudelman, R. Goldston, and R. Kaita, J. Vac. Sci. Technol., 20, 1218 (1982).

[22]S.L. Davis, D. Mueller, and C.J. Keane, Rev. Sci. Instrum. 54, 315 (1983).

Table I

15 Kilogauss Toroidal Field Data

Figure Number	I_p(kA)	P_{abs} (MW)	$T_e(0)$ (eV)	$\bar{n}_e$ ($\times 10^{13}$ cm^{-3})
3a.	250	1.4	700	4.2
3b.	250	2.4	1150	3.7
3c.	250	3.8	1200	3.9
3d.	300	1.0	650	4.2
3e.	300	2.3	1050	3.6
3f.	300	3.3	1250	3.9
3g.	300	4.5	1250	3.3
3h.	350	1.4	700	4.2
3i.	350	2.5	1100	4.5
3j.	350	3.5	1430	4.6
3k.	350	4.5	1300	5.5
3l.	400	1.6	850	4.7
3m.	400	4.1	1320	7.5
3n.	400	5.2	1320	7.5

TABLE II

12 Kilogauss Toroidal Field Data

Figure Number	I_p(kA)	P_{abs} (MW)	$T_e(0)$ (eV)	$\bar{n}_e$ ($\times 10^{13}$ cm^{-3})
4a.	250	1.3	740	3.5
4b.	250	2.4	850	3.7
4c.	250	4.1	750	3.7
4d.	250	5.0	950	3.4
4e.	300	1.0	700	3.7
4f.	300	2.7	900	3.4
4g.	300	3.5	900	3.7
4h.	300	5.2	875	3.8
4i.	350	1.5	750	3.4
4j.	350	2.5	750	3.3
4k.	350	3.6	1100	3.7
4l.	350	5.0	1050	4.2
4m.	400	1.5	828	3.7
4n.	400	2.3	930	3.9
4o.	400	3.5	1130	4.2
4p.	400	4.7	1220	4.8

FIGURE CAPTIONS

FIG. 1 Layout of PDX, showing the relative positions of the four near-perpendicular neutral beam injectors, the horizontally scanning neutral particle analyzer, and the limiters used for circular plasmas.

FIG. 2 Slowing-down spectrum for one deuterium beam in a 22-kG, 380-kA deuterium (limiter) plasma. The dashed curves were obtained from a bounce-averaged Fokker-Planck calculation.

FIG. 3a)-3n) Slowing-down spectra for deuterium injection in a 15-kG hydrogen limiter plasma. The plasma conditions associated with each spectrum are listed in Table I, and the absolute units for the ordinate are described in Ref. 22. For these MHD-quiescent plasmas, the magnitude of the spectra varies linearly with increasing beam power.

FIG. 4a)-4p) Slowing-down spectra for deuterium injection in a 12-kG hydrogen limiter plasma. The plasma conditions associated with each spectrum are listed in Table II. At the highest beam powers for the 400 kA plasmas, the strong onset of the fishbone instability keeps the spectra from scaling with the number of beams.

FIG. 5a) - 5b) Average fast ion flux between the injection energy and half the injection energy, as a function of absorbed beam power, for the data displayed in Figs. 3 and 4, respectively.

FIG. 5c) - 5d) Particle confinement time, as a function of absorbed beam power, for the data displayed in Figs. 3 and 4, respectively.

FIG. 6 Measured fast neutral flux as a function of time during an H-mode discharge. Note the rapid drop in the signal when the transition occurs.

FIG. 7 Measured percentage of neutral particles versus horizontal transverse distance across the Northwest neutral heating beam (Fig. 1).

FIG. 8 Beam distribution spatial zones used in the transport analysis and beam simulation code TRANSP.

FIG. 9 Schematic of sightline tracking algorithm in TRANSP.

FIG. 10 Comparison between the predictions of the bounce-averaged Fokker-Planck code (dashed curves) and the TRANSP simulation program (solid curves), with both the toroidal field and plasma current set arbitrarily high in each case.

FIG. 11 Slowing-down spectrum for one deuterium beam in a deuterium plasma, as in Fig. 2, compared with results (dashed curves) from the TRANSP simulation calculation.

FIG. 12 Slowing-down spectrum for two deuterium beams in a 10-kG, 280-kA hydrogen (divertor) plasma. The TRANSP Monte-Carlo results (dashed curves) agree both in shape and absolute magnitude with the experimental data.

FIG. 13 Slowing-down spectrum for deuterium beams in a 17.7-kG, 350-kA deuterium scoop limiter plasma. The dashed curves are from the TRANSP Monte-Carlo model using a toroidally averaged wall neutrals source and only the agreement in absolute magnitude with the most perpendicular channel is good.

FIG. 14 Results from a bounce-averaged Fokker-Planck calculation (solid curves) with the scoop simulated by a toroidally local point neutrals source, and a TRANSP spectrum (dashed curves) assuming a toroidally averaged volume source of neutrals.

FIG. 15 Slowing-down spectrum for deuterium beams in a 17.7-kG, 350-kA deuterium scoop limiter plasma. The dashed curves are from a TRANSP calculation using a toroidally averaged volume source of neutrals, and the agreement with the flux measured along successive sightlines is improved.

FIG. 16 Slowing-down spectrum for two deuterium beams in a 17-kG, 350-kA H-mode deuterium (divertor) plasma. The TRANSP results are shown as dashed curves on the plot.

FIG. 17 Slowing-down spectrum for four deuterium counter beams in an 8.4-kG, 295-kA hydrogen (limiter) plasma. The dashed curves are from a TRANSP calculation, in which radial excursions of beam ions into the region of high neutral density beyond the plasma minor radius, where charge-exchange losses are likely to occur, are allowed.

FIG. 18 Slowing-down spectrum for the East deuterium beam (Fig. 1) in a 12-kG, 300-kA hydrogen (limiter) plasma. This beam is closest toroidally to the neutral particle analyzer, and thus has the largest "prompt" peaks at the full, half, and third energies.

FIG. 19 Height of the full energy peak from successive one beam slowing-down spectra as a function of toroidal distance from the neutral particle analyzer.

FIG. 20 Calculated first "half-orbits" for low current counter-injection.

FIG. 21a) Charge-exchange flux during deuterium counter-injection in a 350-kA deuterium scoop limiter discharge. At a tangency radius of 70 cm, the analyzer viewed co-moving particles on the outer leg of outer region loss orbits (Fig. 20). Since the deflection voltage of the analyzer is swept as a function of time, the "normal" edge loss peak is seen when the corresponding detection energy passes through the neutral beam injection energy.

b) At a more tangential angle, the charge-exchange signal rises at the time the voltage sweep reaches the neutral beam injection energy, and shows the decrease below this energy characteristic of a "normal" slowing-down spectrum.

c) At a still more tangential angle, a sharp rise in the charge-exchange signal is seen again at the injection energy, which corresponds to the "new" central loss peak described in the text.

FIG. 22 Amplitude of the prompt charge-exchange loss peak near the injection energy as a function of analyzer aiming radius. The existence of a second peak at an angle much more parallel than the injection angle is consistent with the central loss orbits in Fig. 20.

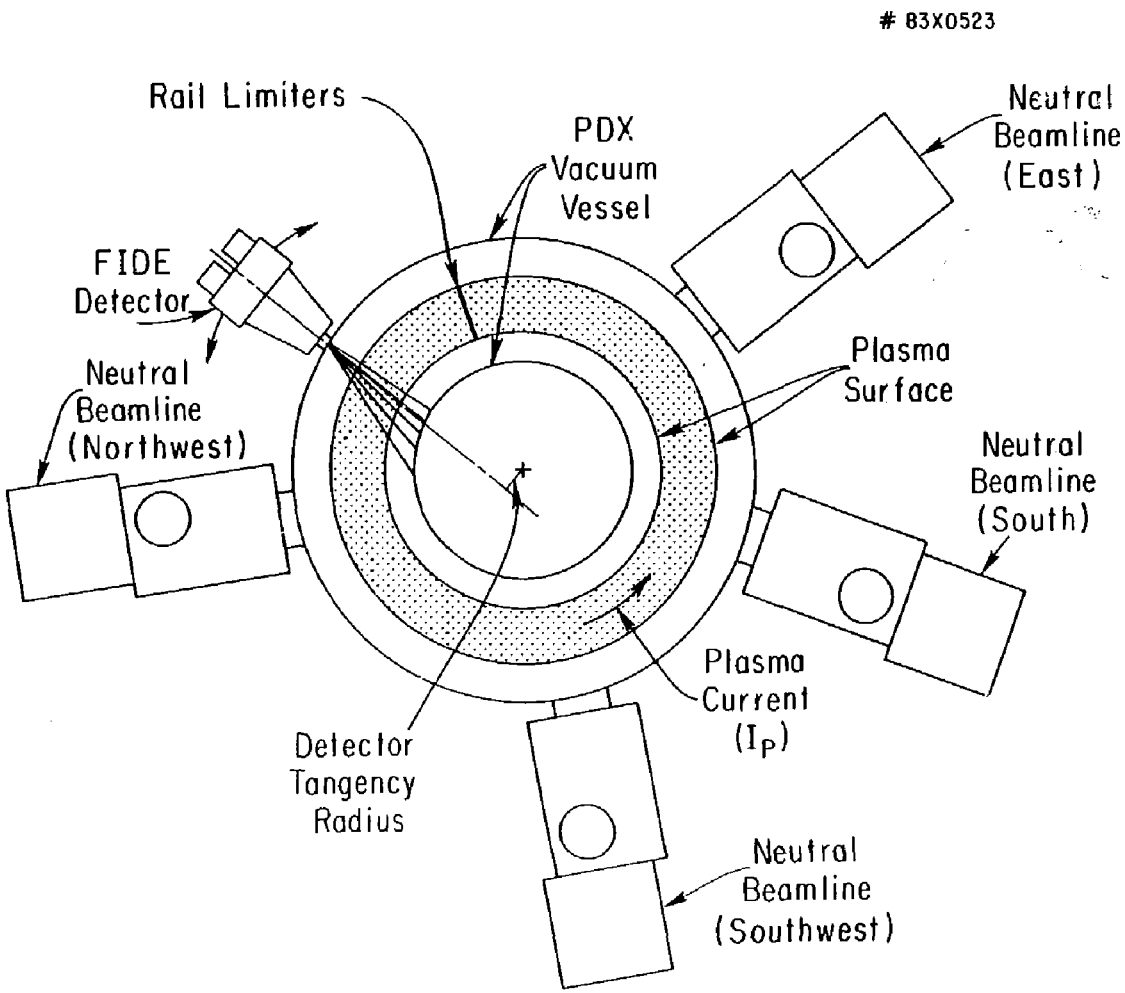
83X0523
Rail Limiters
PDX
Vacuum
Vessel
Neutral
Beamline
(East)
FIDE
Detector
Neutral
Beamline
(Northwest)
Plasma
Surface
Neutral
Beamline
(South)
Plasma
Current
(I_P)
Detector
Tangency
Radius
Neutral
Beamline
(Southwest)

Fig. 1

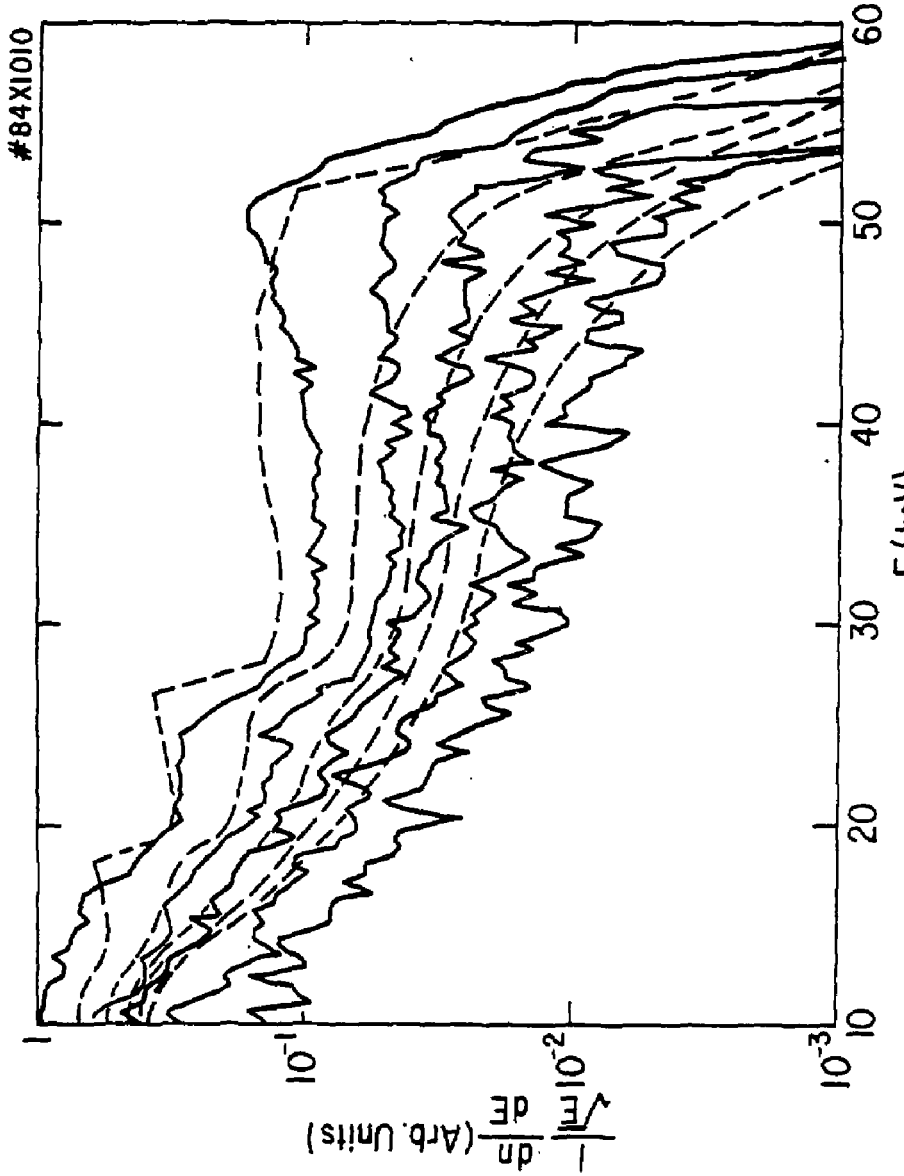
#84X1010
$\frac{1}{\sqrt{E}}\frac{dn}{dE}$(Arb. Units)
10^{-1}
10^{-2}
10^{-3}
10
20
30
40
50
60
E (keV)

Fig. 2

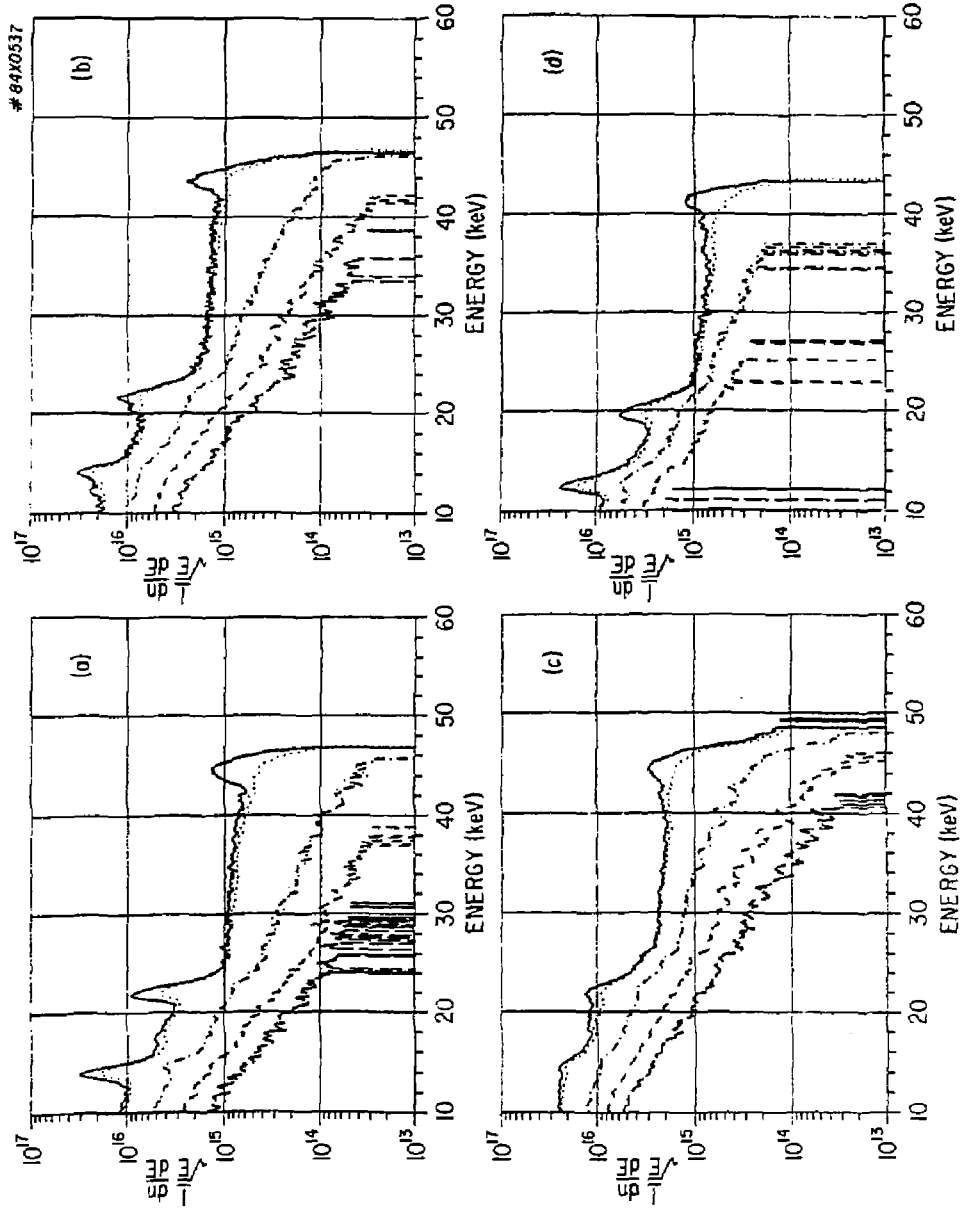

Fig. 3 (a-d)

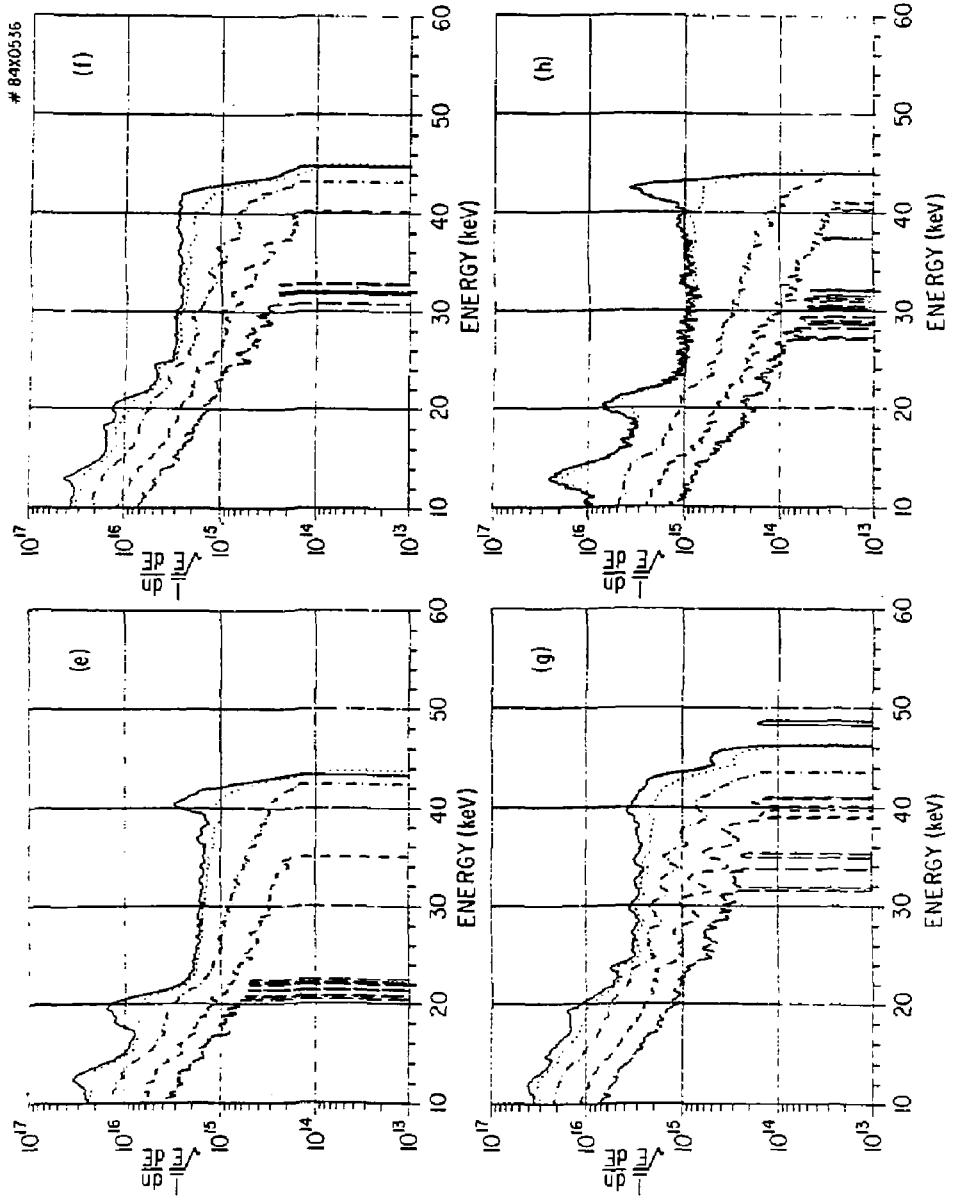

Fig. 3 (e-h)

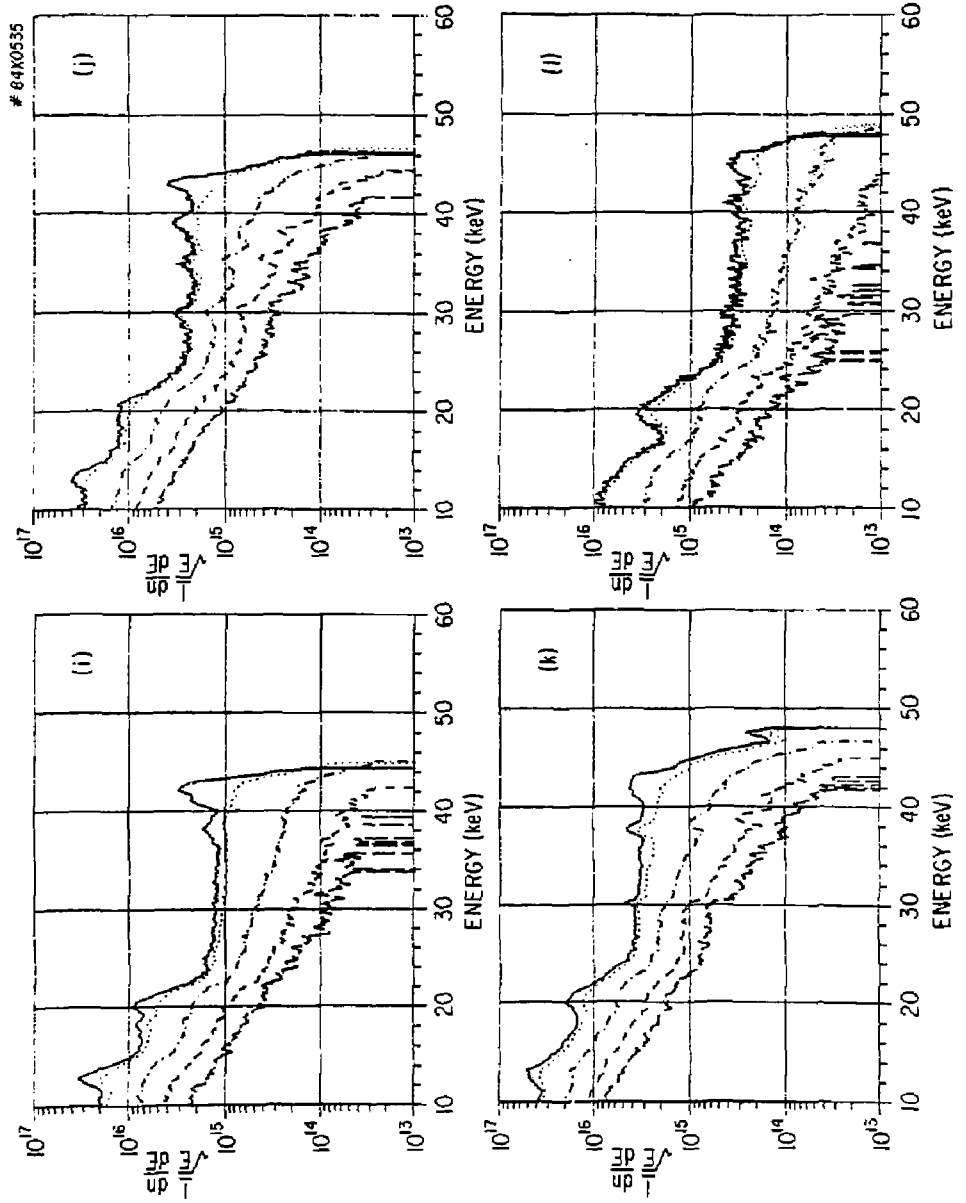

Fig. 3 (i-l)

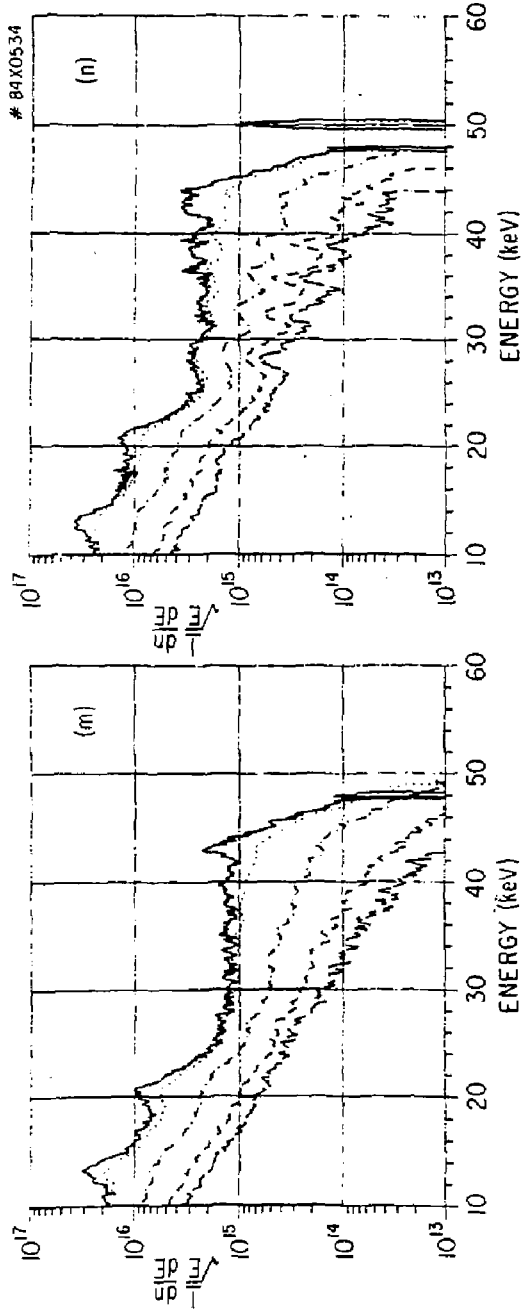

Fig. 3 (m-n)

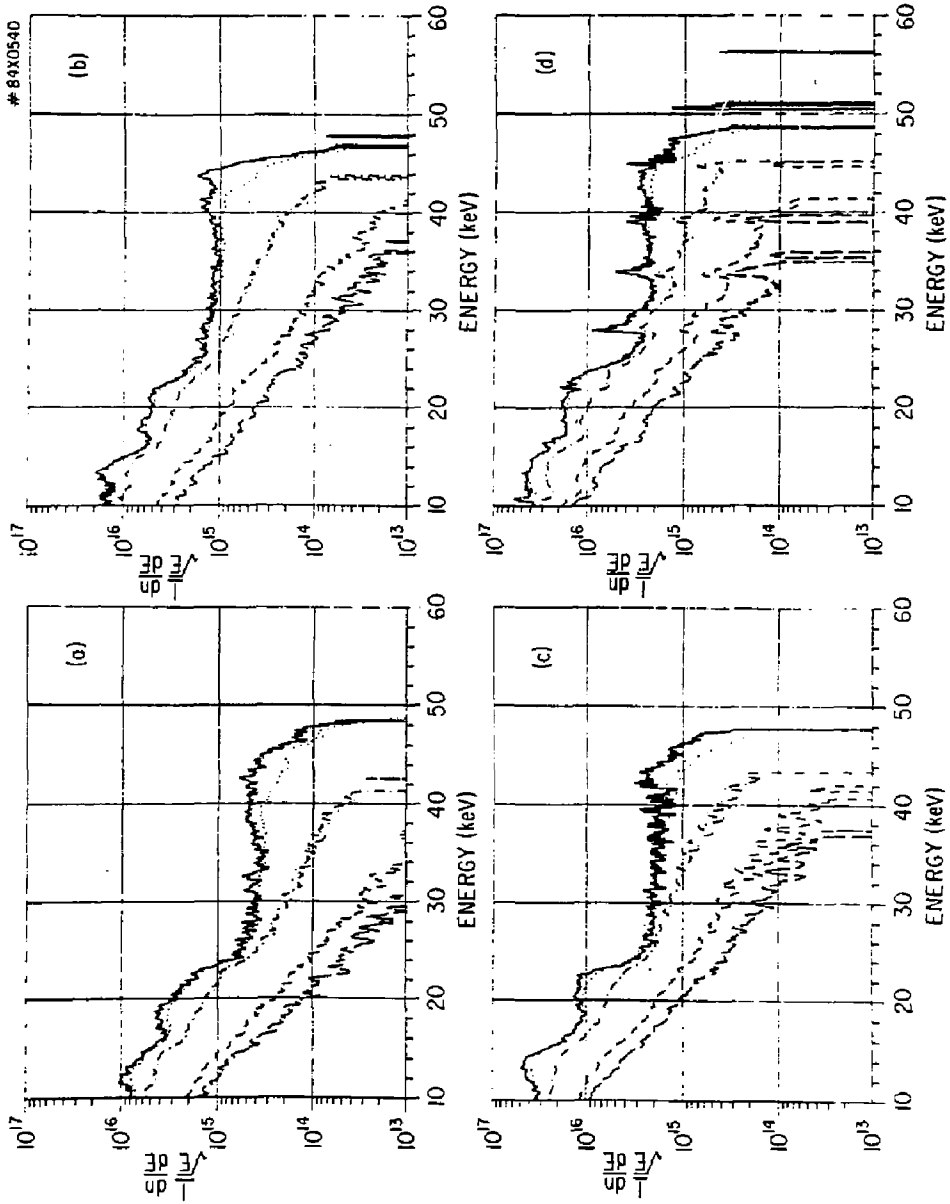

Fig. 4 (a-d)

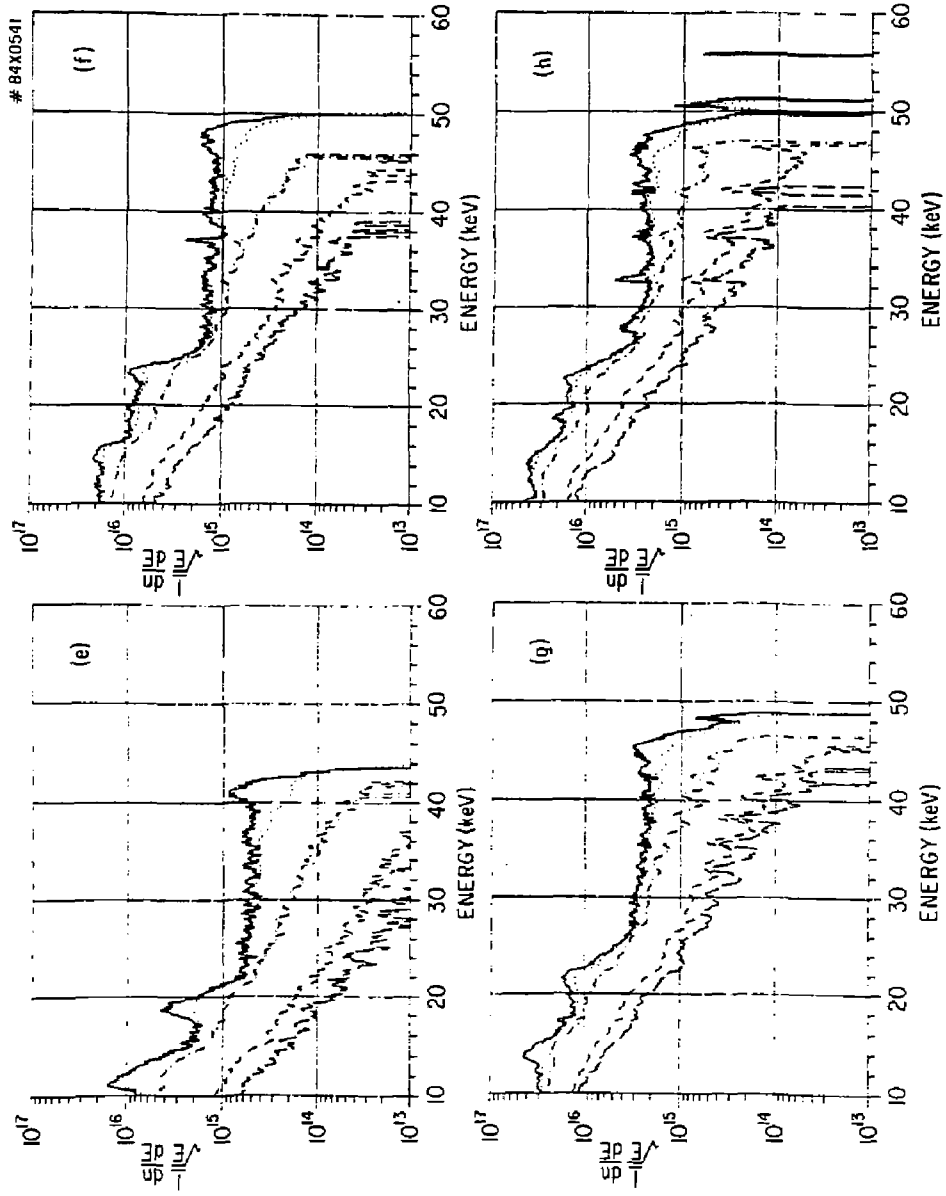
84X0541
(e)
(f)
(g)
(h)
$\sqrt{E}\frac{dn}{dE}$
ENERGY (keV)
10^{17}
10^{16}
10^{15}
10^{14}
10^{13}
10
20
30
40
50
60

Fig. 4 (e-h)

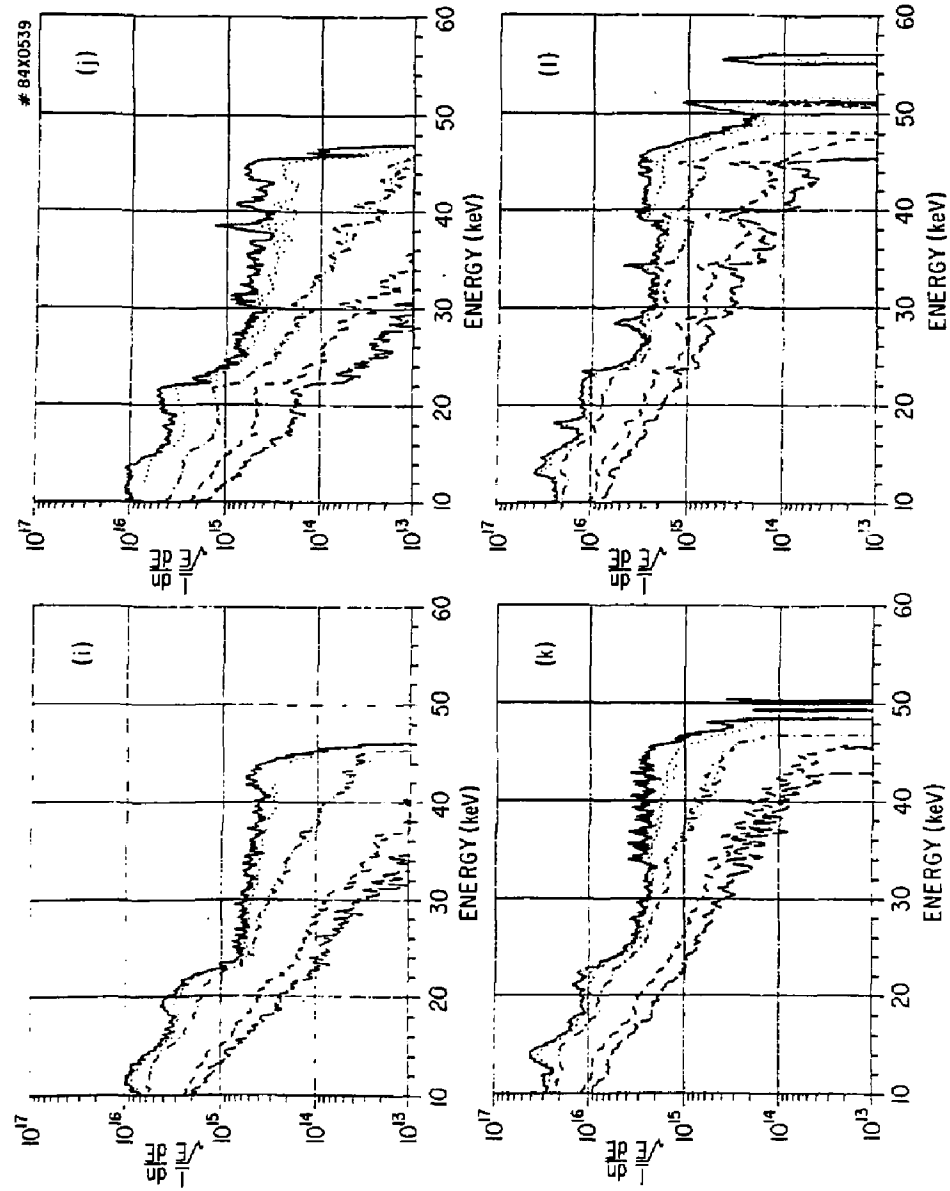

Fig. 4 (i-l)

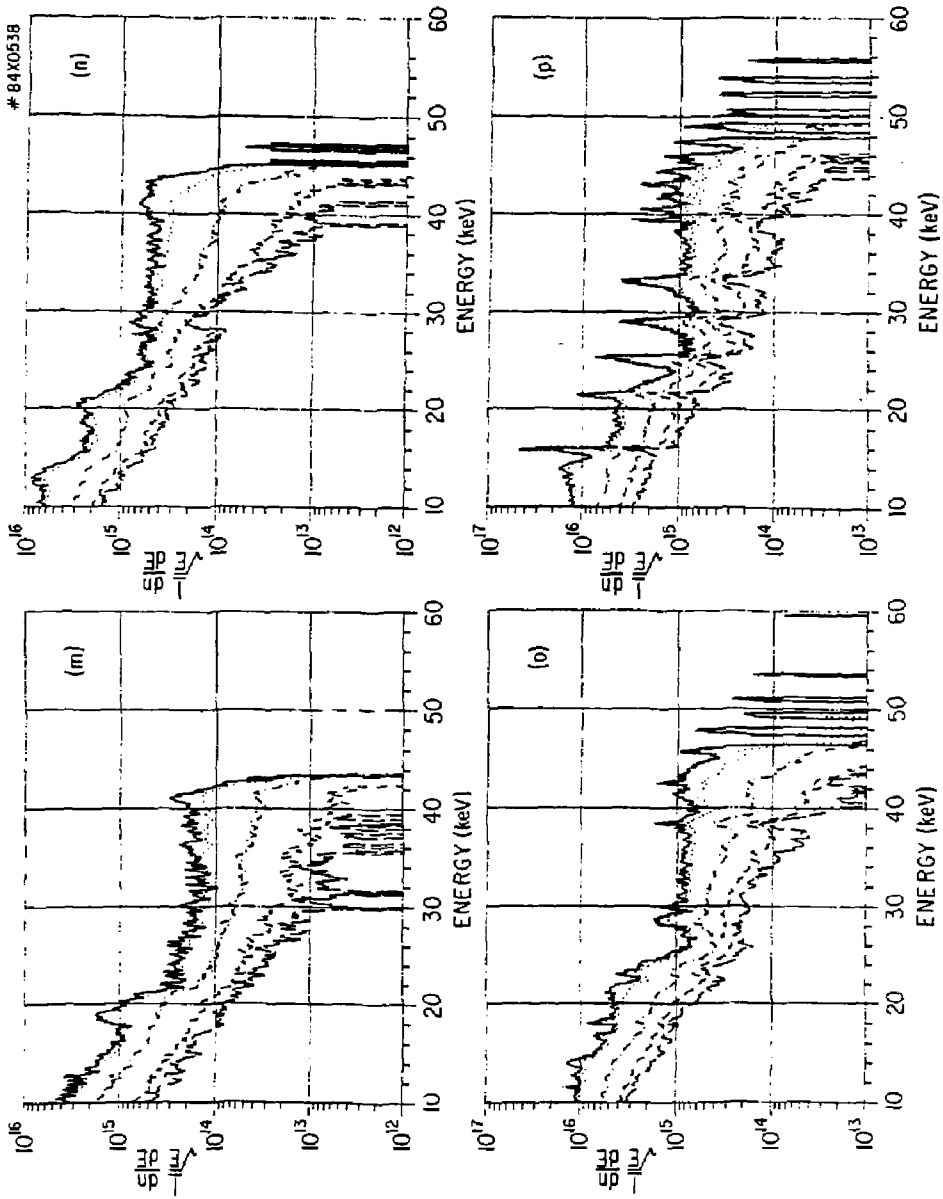

Fig. 4 (m-p)

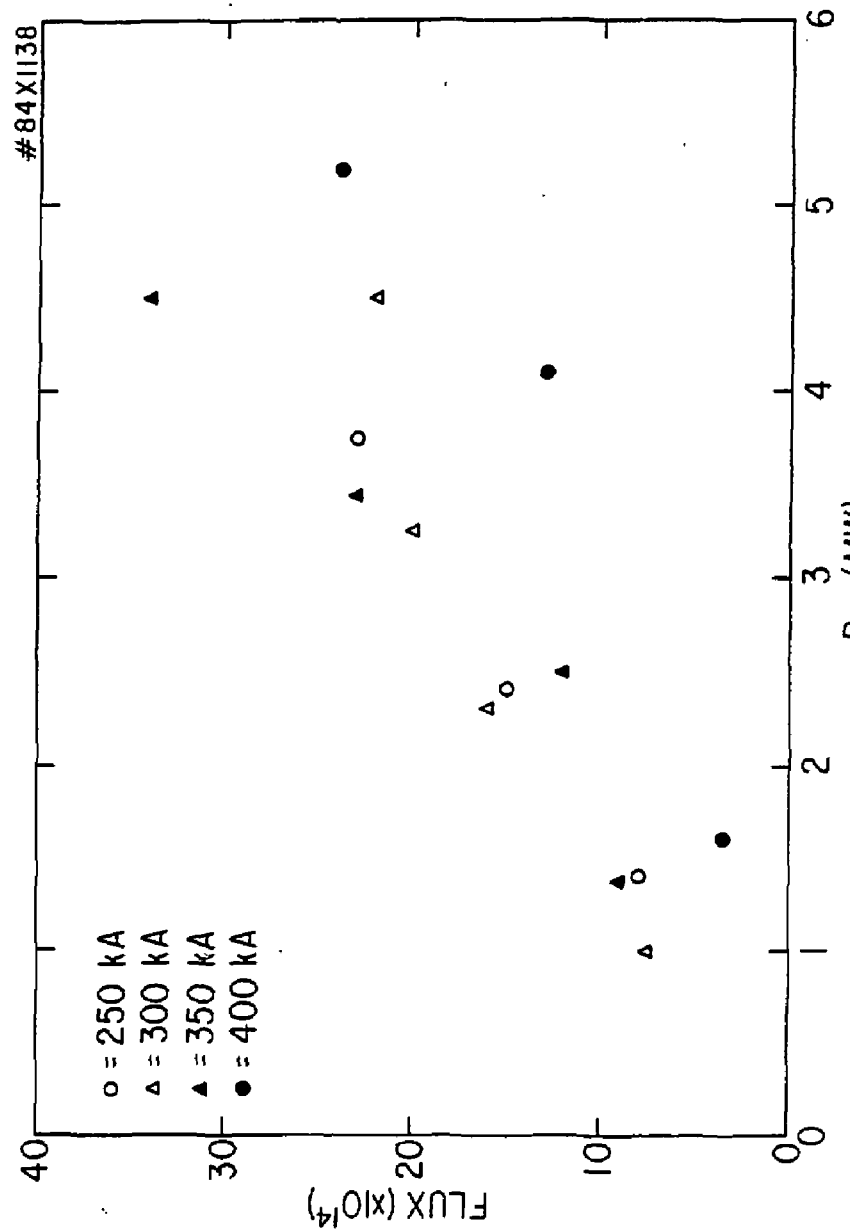
#84X1138
o = 250 kA
Δ = 300 kA
▲ = 350 kA
● = 400 kA
FLUX (x10¹⁴)
0
10
20
30
40
0
1
2
3
4
5
6
P_{ABS}(MW)

Fig. 5 (a)

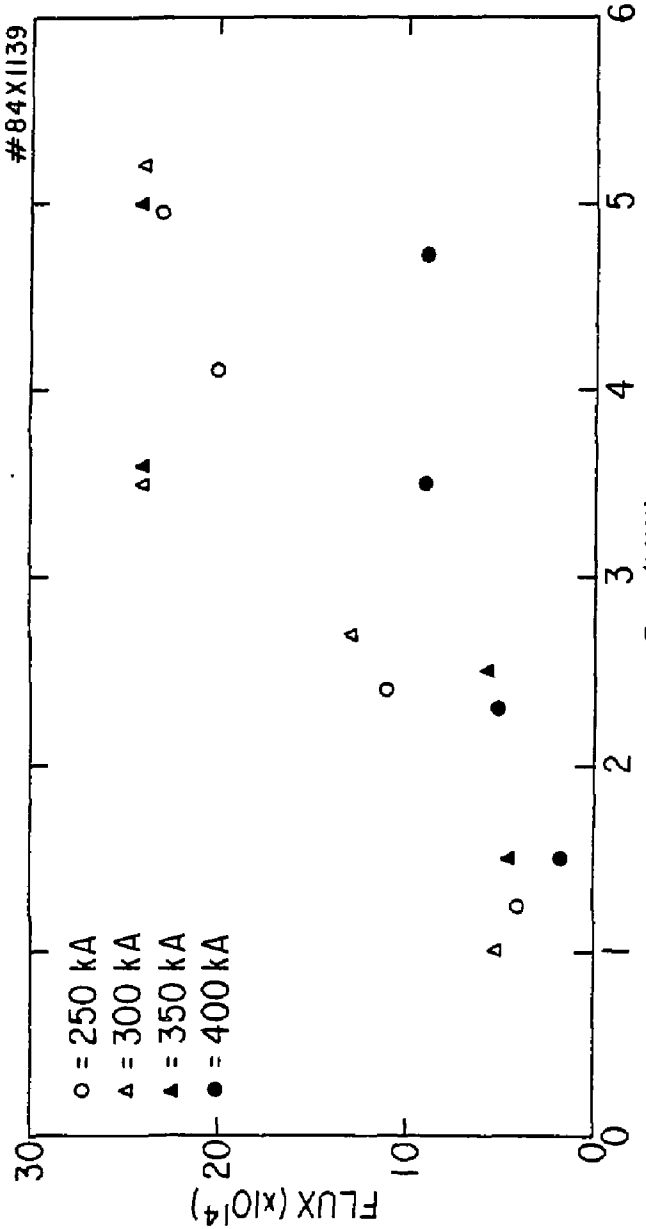
#84X1139
o = 250 kA
Δ = 300 kA
▲ = 350 kA
● = 400 kA
FLUX (x10¹⁴)
P_ABS (MW)
0
10
20
30
1
2
3
4
5
6

Fig. 5 (b)

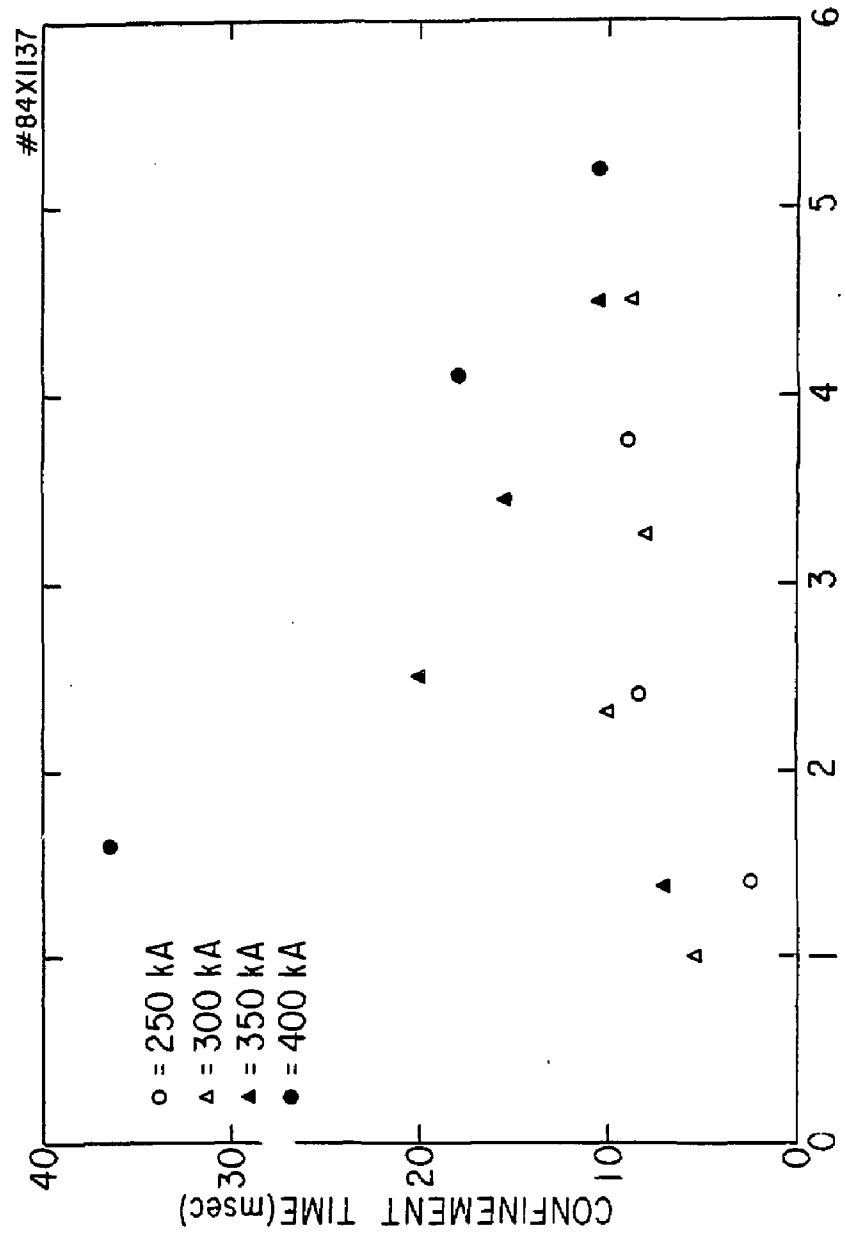
#84X1137
CONFINEMENT TIME(msec)
P_{ABS}(MW)
o = 250 kA
Δ = 300 kA
▲ = 350 kA
● = 400 kA
0
10
20
30
40
1
2
3
4
5
6

Fig. 5(a)

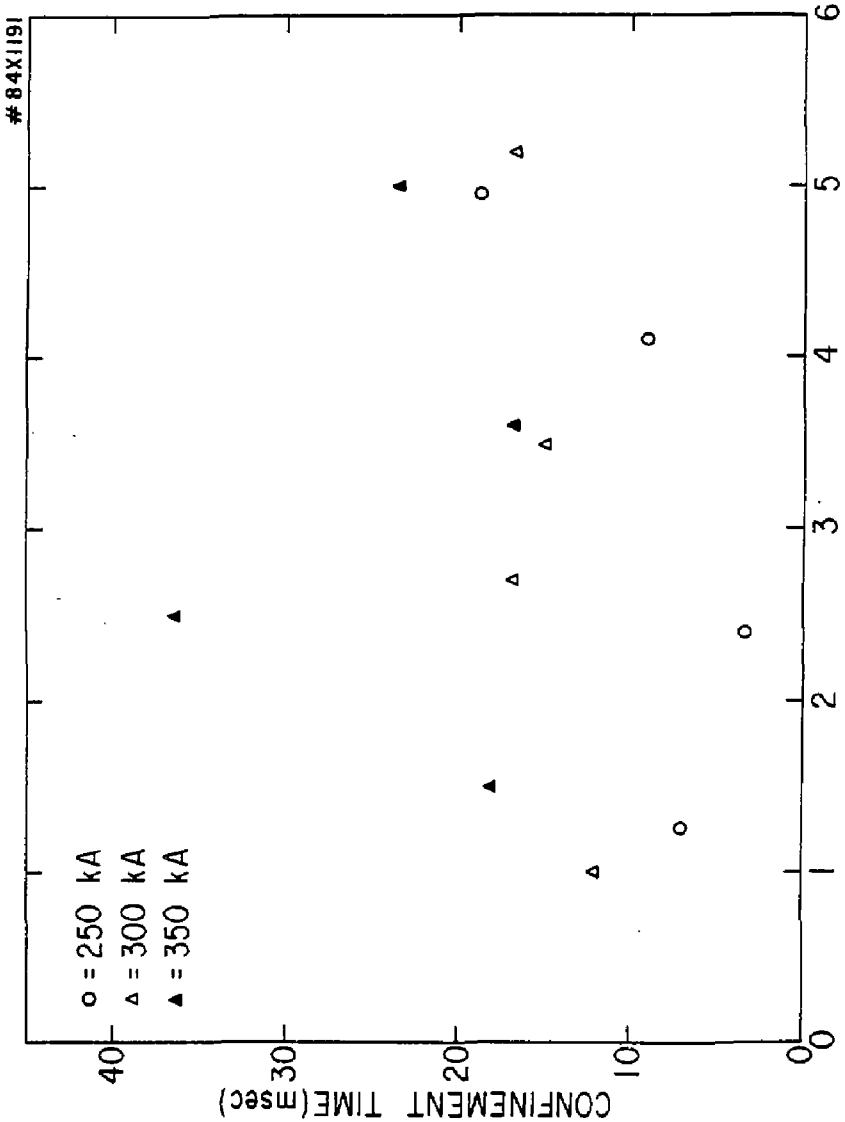
#84X1191
o = 250 kA
Δ = 300 kA
▲ = 350 kA
CONFINEMENT TIME (msec)
0
10
20
30
40
0
1
2
3
4
5
6
P_{ABS} (MW)

Fig. 5 (d)

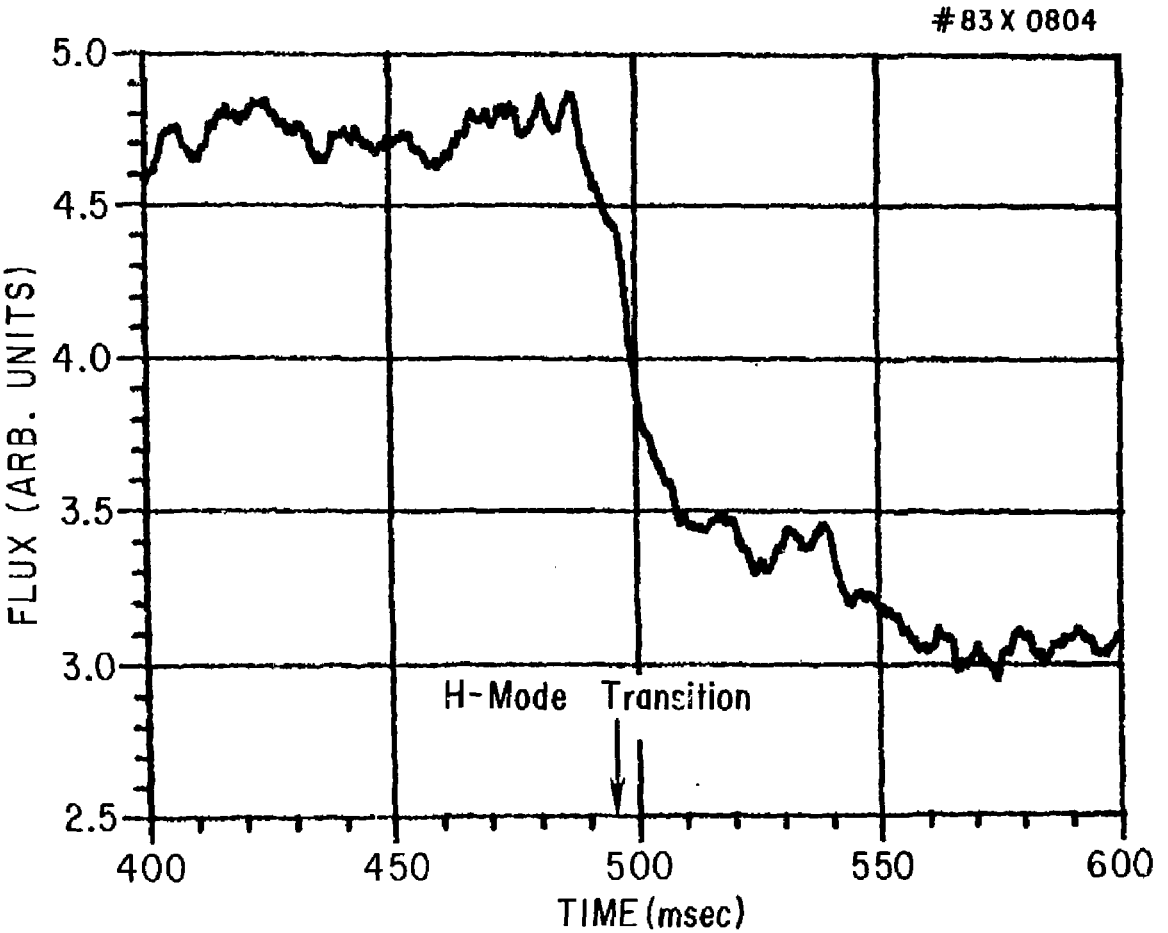
#83X 0804
5.0
4.5
4.0
3.5
3.0
2.5
FLUX (ARB. UNITS)
H-Mode Transition
400
450
500
550
600
TIME (msec)

Fig. 6

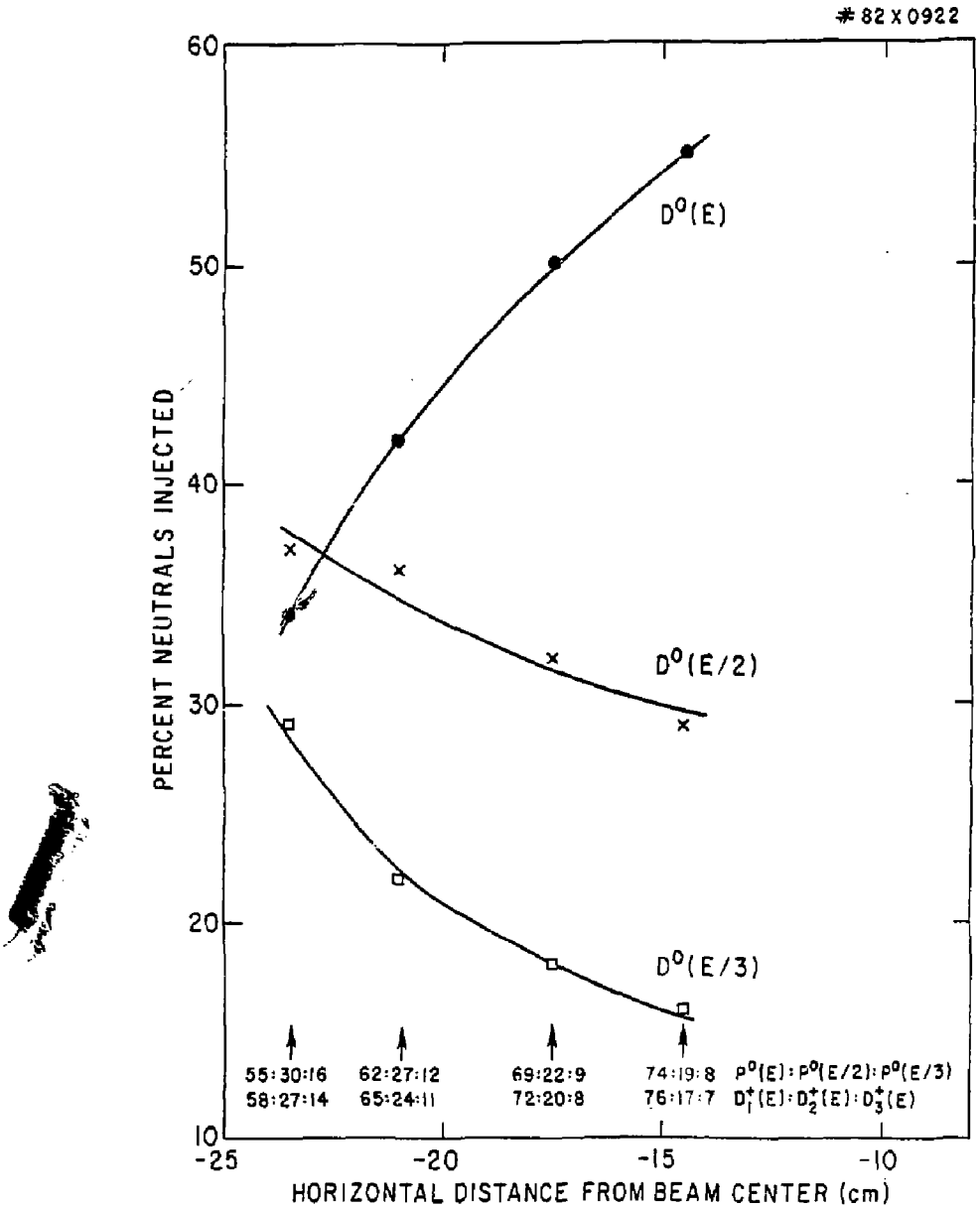
#82X0922
60
50
40
30
20
10
PERCENT NEUTRALS INJECTED
D⁰(E)
D⁰(E/2)
D⁰(E/3)
55:30:16
58:27:14
62:27:12
65:24:11
69:22:9
72:20:8
74:19:8
76:17:7
P⁰(E):P⁰(E/2):P⁰(E/3)
D₁⁺(E):D₂⁺(E):D₃⁺(E)
-25
-20
-15
-10
HORIZONTAL DISTANCE FROM BEAM CENTER (cm)

Fig. 7

#82X0926

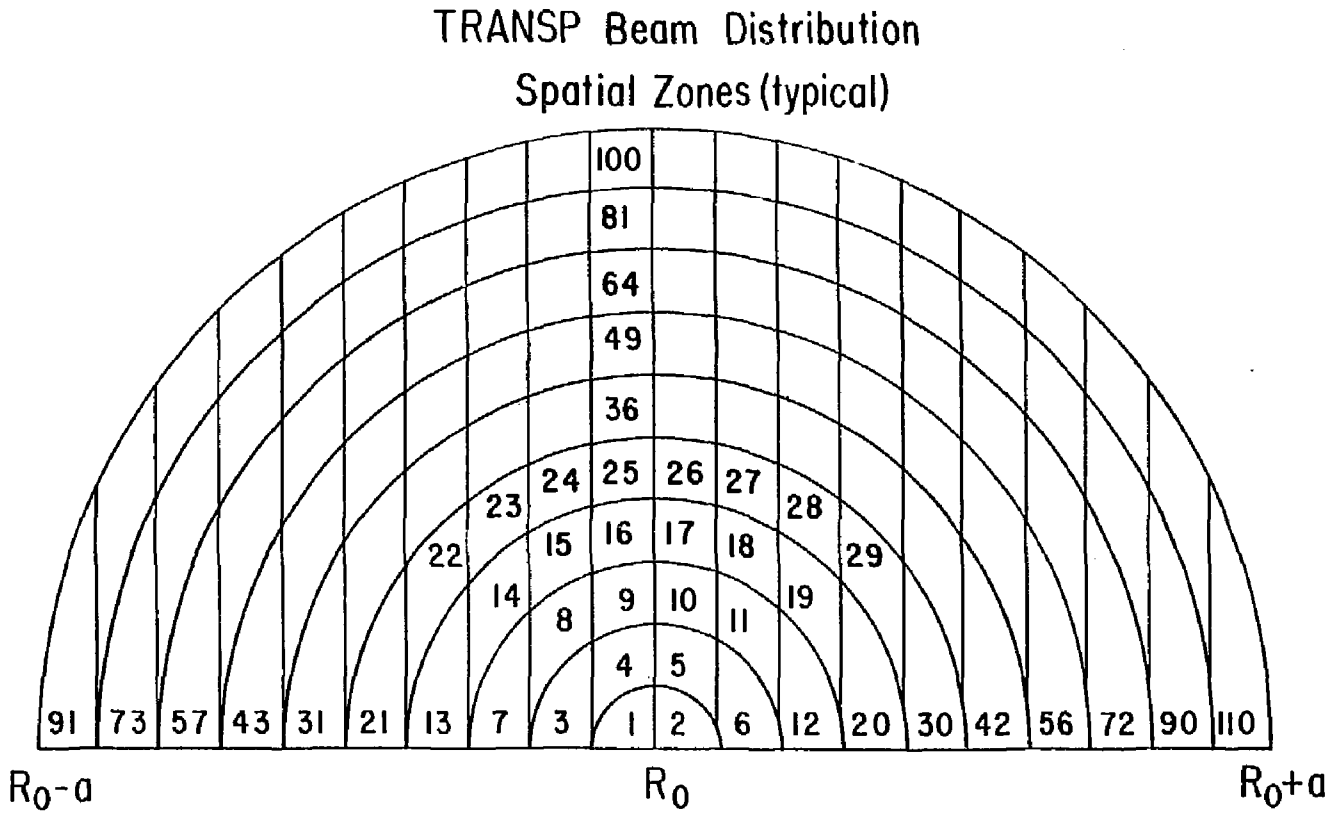

Fig. 8

#82X0930

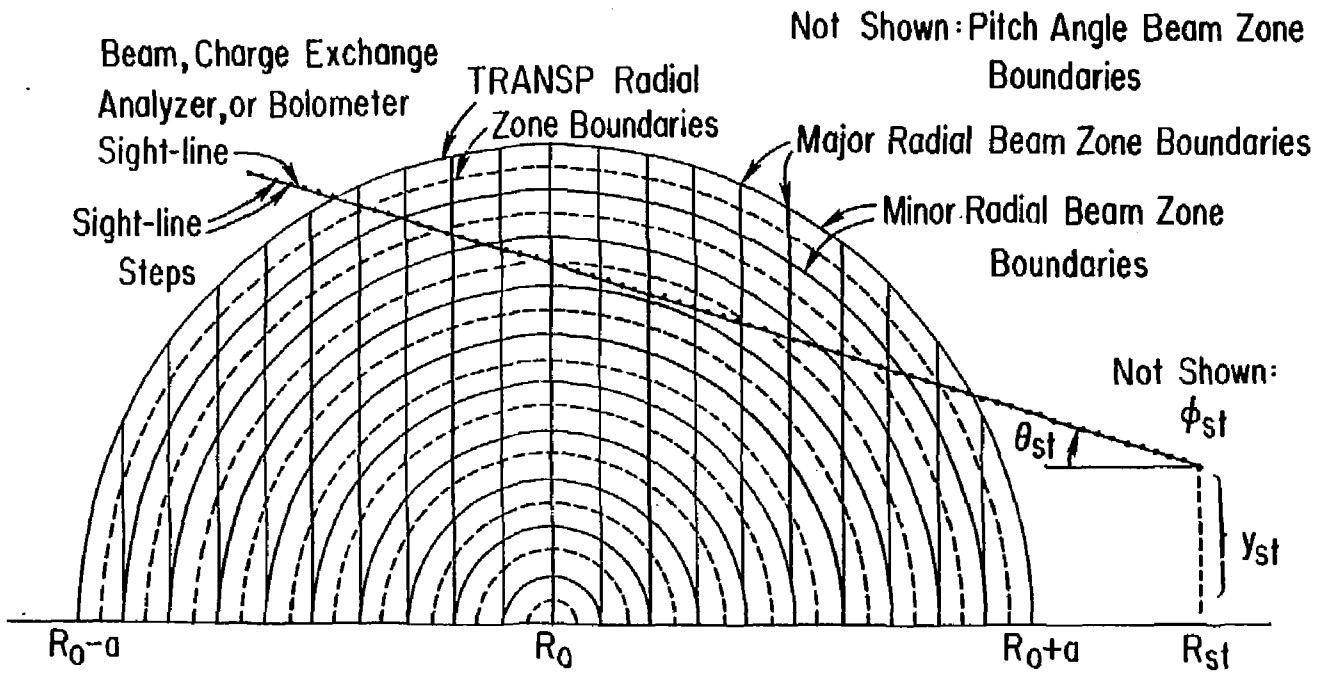

Fig. 9

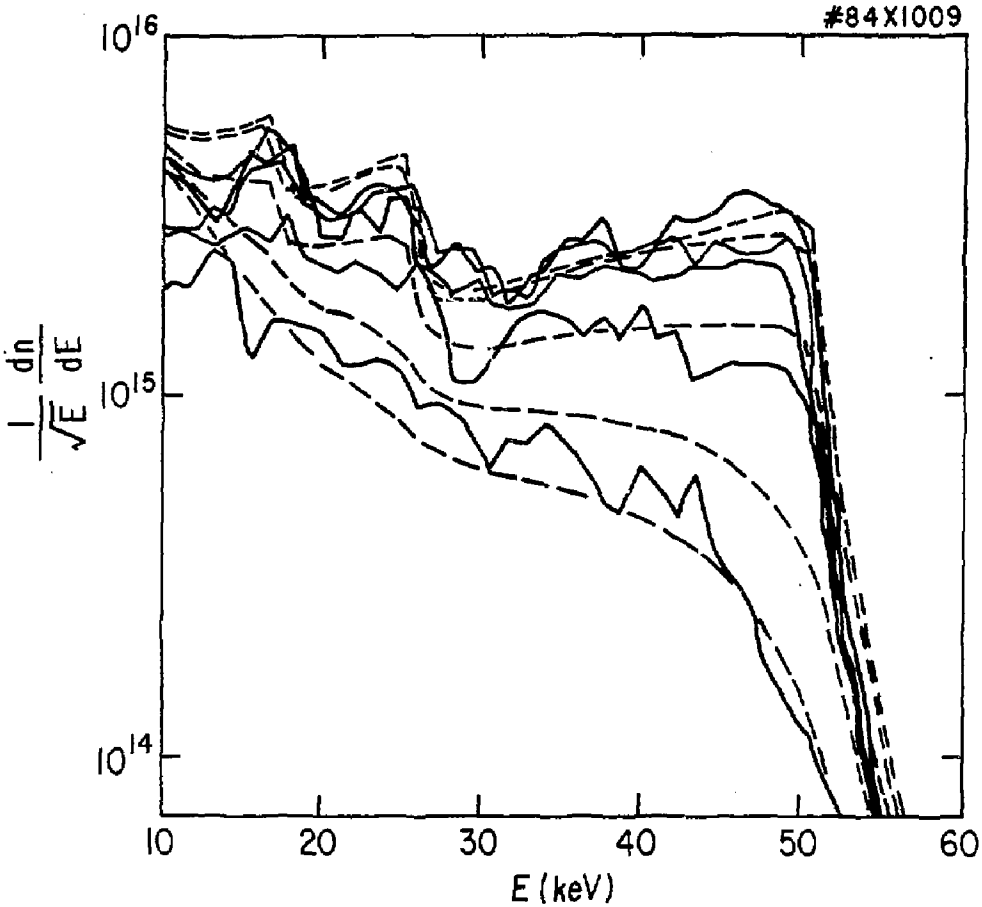
#84X1009
10^{16}
10^{15}
10^{14}
$\frac{1}{\sqrt{E}}\frac{dn}{dE}$
10
20
30
40
50
60
E (keV)

Fig. 10

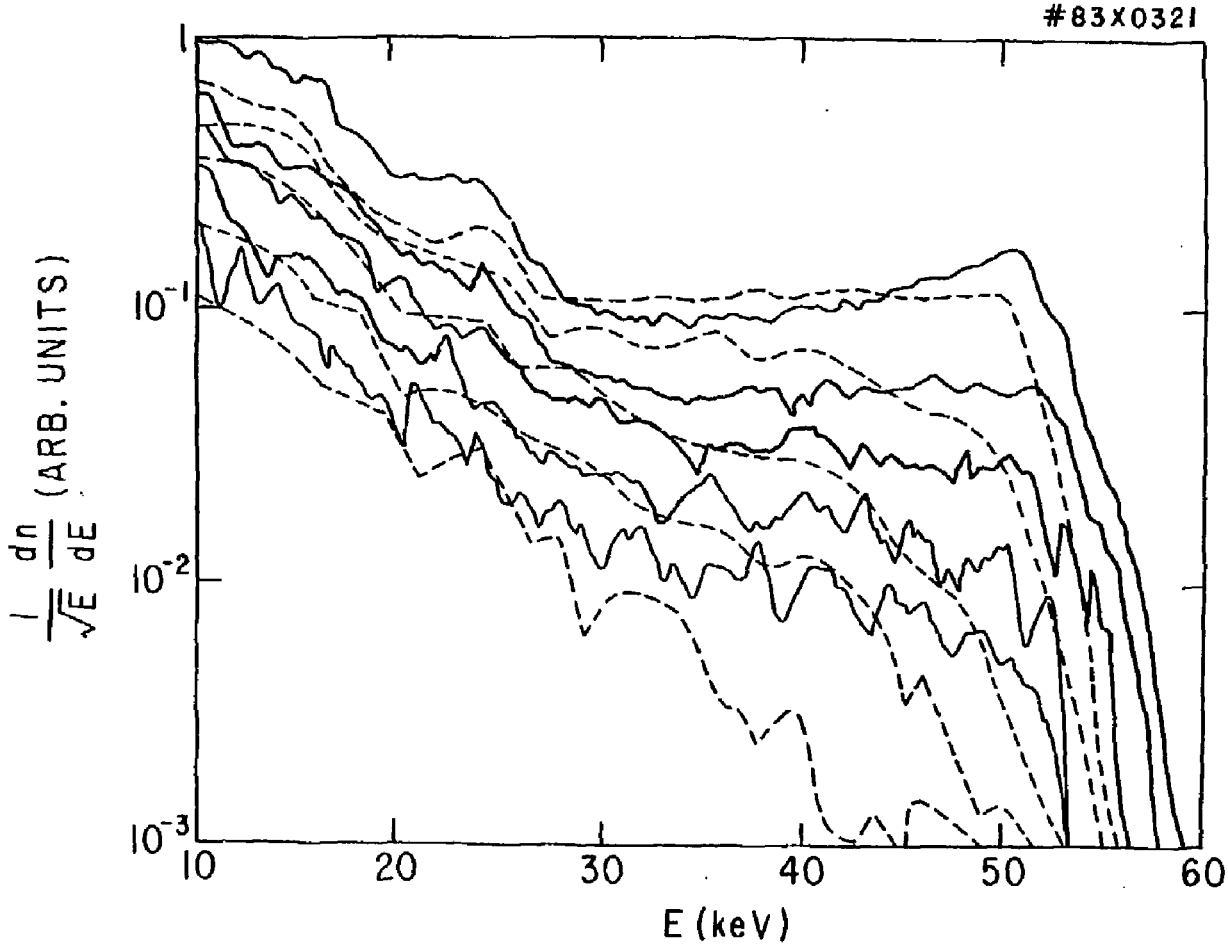
#83X0321
1
10^{-1}
10^{-2}
10^{-3}
$\frac{1}{\sqrt{E}}\frac{dn}{dE}$ (ARB. UNITS)
10
20
30
40
50
60
E (keV)

Fig. 11

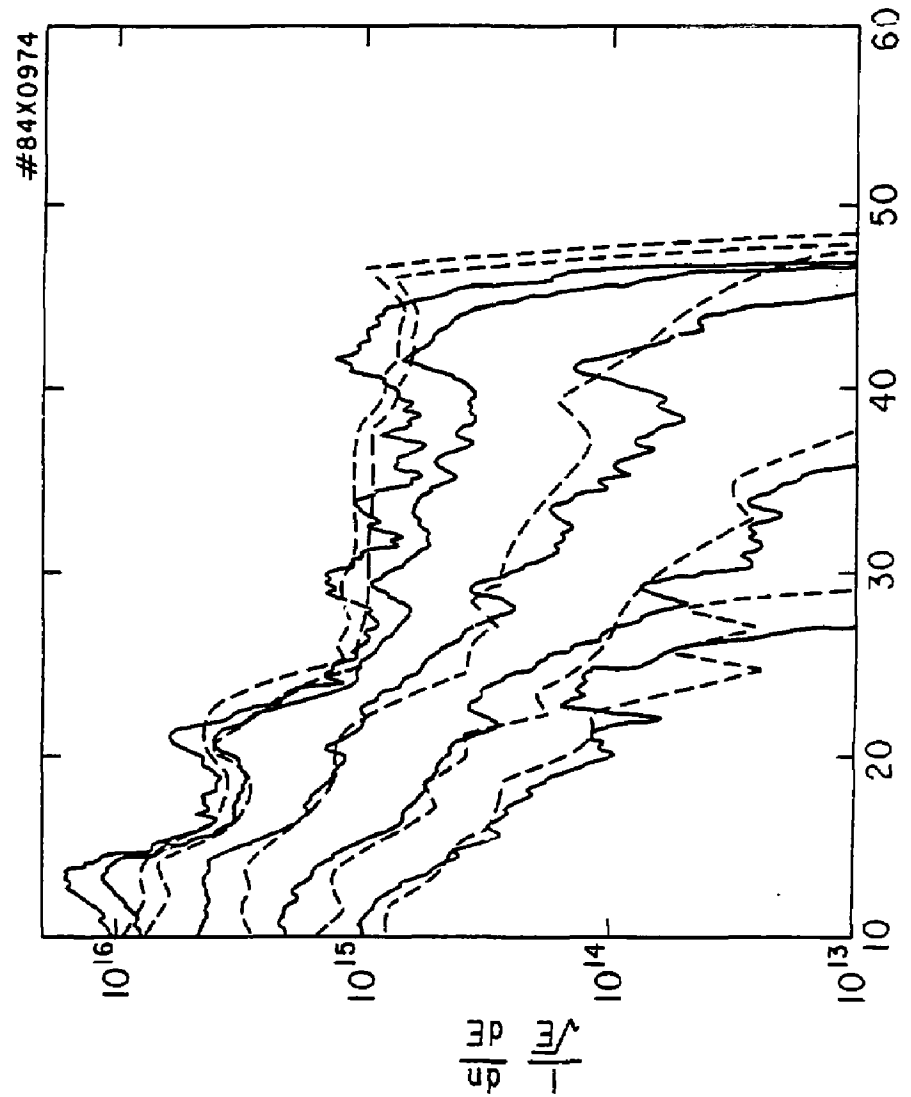
#84X0974
$\frac{1}{\sqrt{E}} \frac{dn}{dE}$
10^{16}
10^{15}
10^{14}
10^{13}
10
20
30
40
50
60
E(keV)

Fig. 12

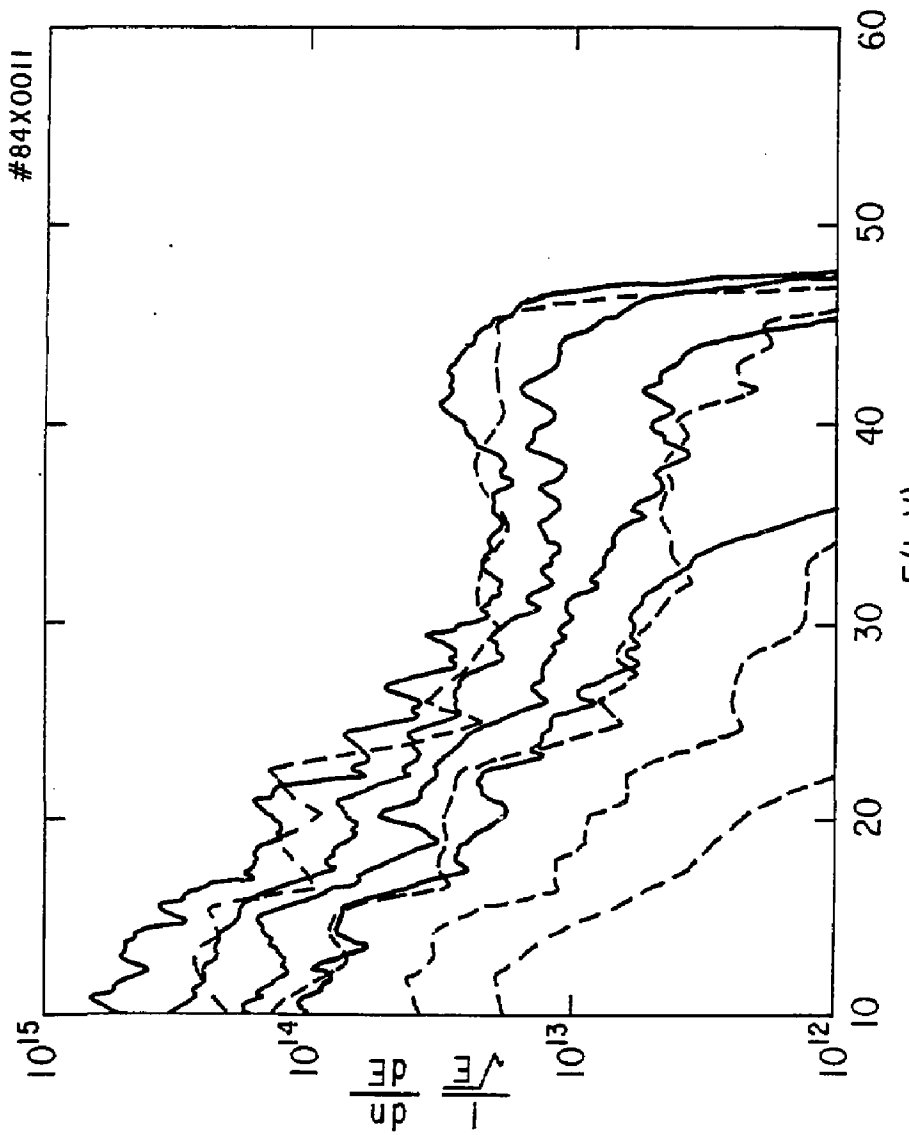
#84X0011
10^{15}
10^{14}
10^{13}
10^{12}
$\frac{1}{\sqrt{E}} \frac{dn}{dE}$
10
20
30
40
50
60
E (keV)

Fig. 13

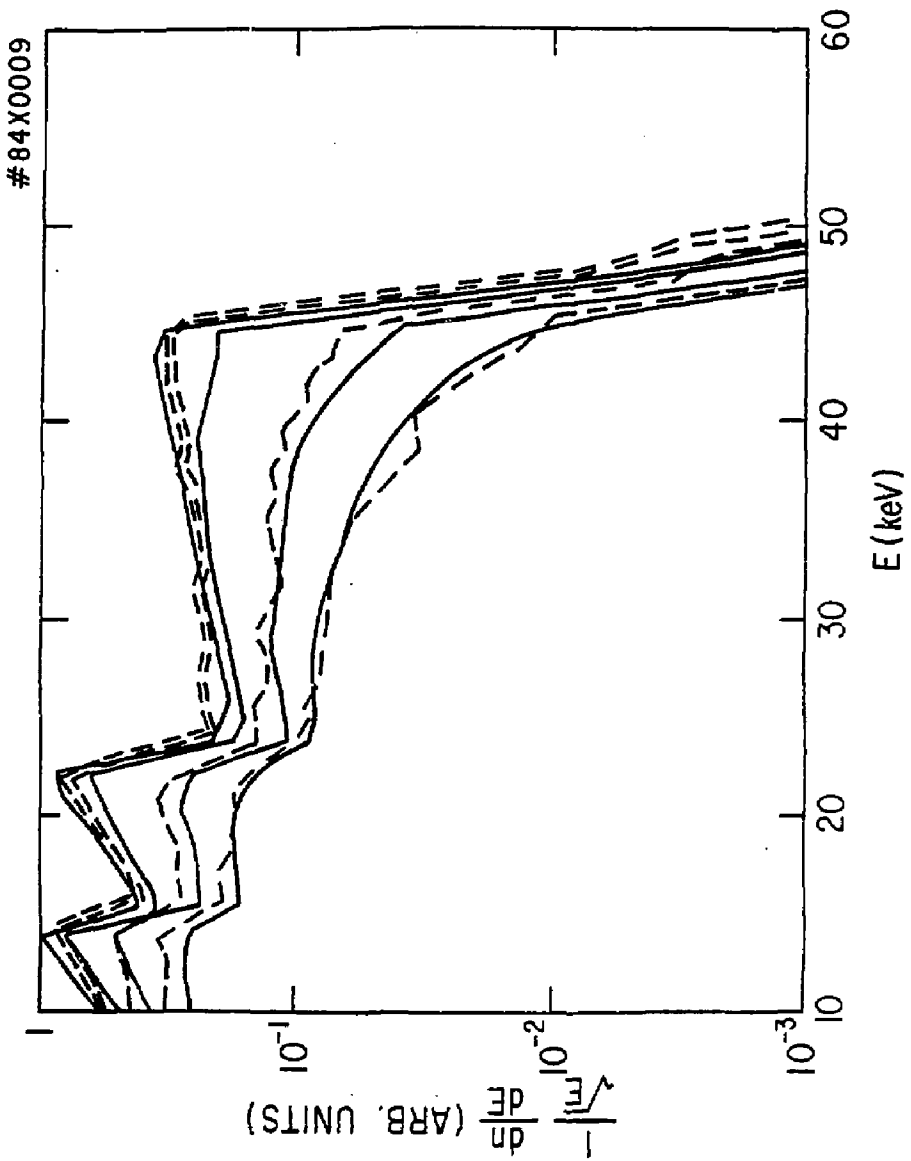
#84X0009
$\frac{1}{\sqrt{E}}\frac{dn}{dE}$ (ARB. UNITS)
10^{-1}
10^{-2}
10^{-3}
10
20
30
40
50
60
E(keV)

Fig. 14

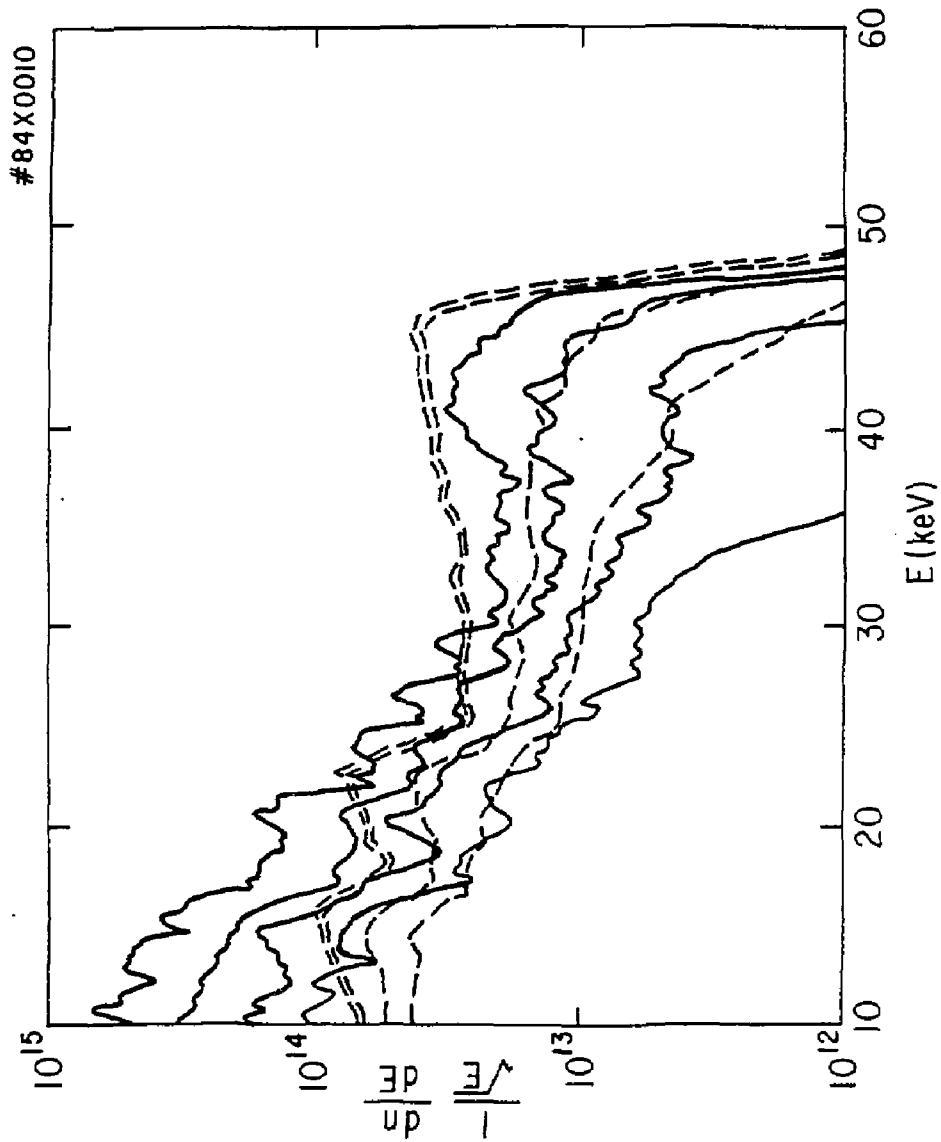
#84X0010
10^{15}
10^{14}
10^{13}
10^{12}
$\frac{1}{\sqrt{E}} \frac{dn}{dE}$
10
20
30
40
50
60
E (keV)

Fig. 15

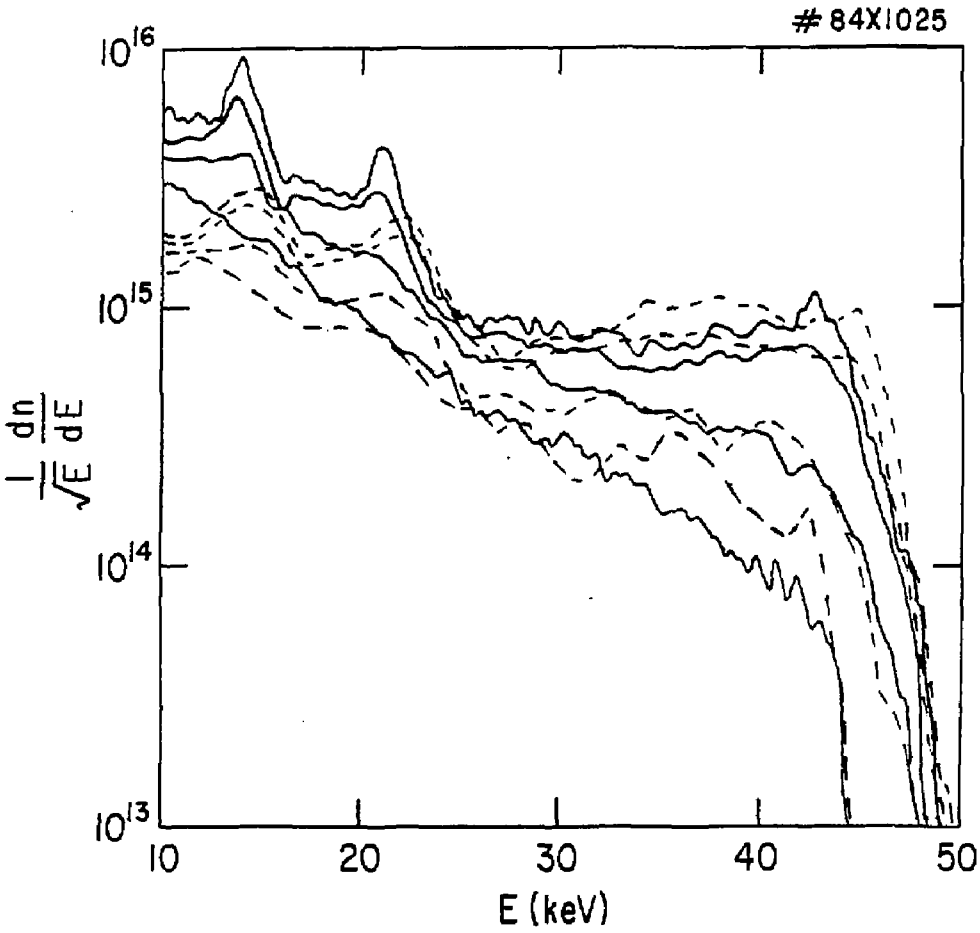
#84X1025
10^{16}
10^{15}
10^{14}
10^{13}
$\frac{1}{\sqrt{E}}\frac{dn}{dE}$
10
20
30
40
50
E (keV)

Fig. 16

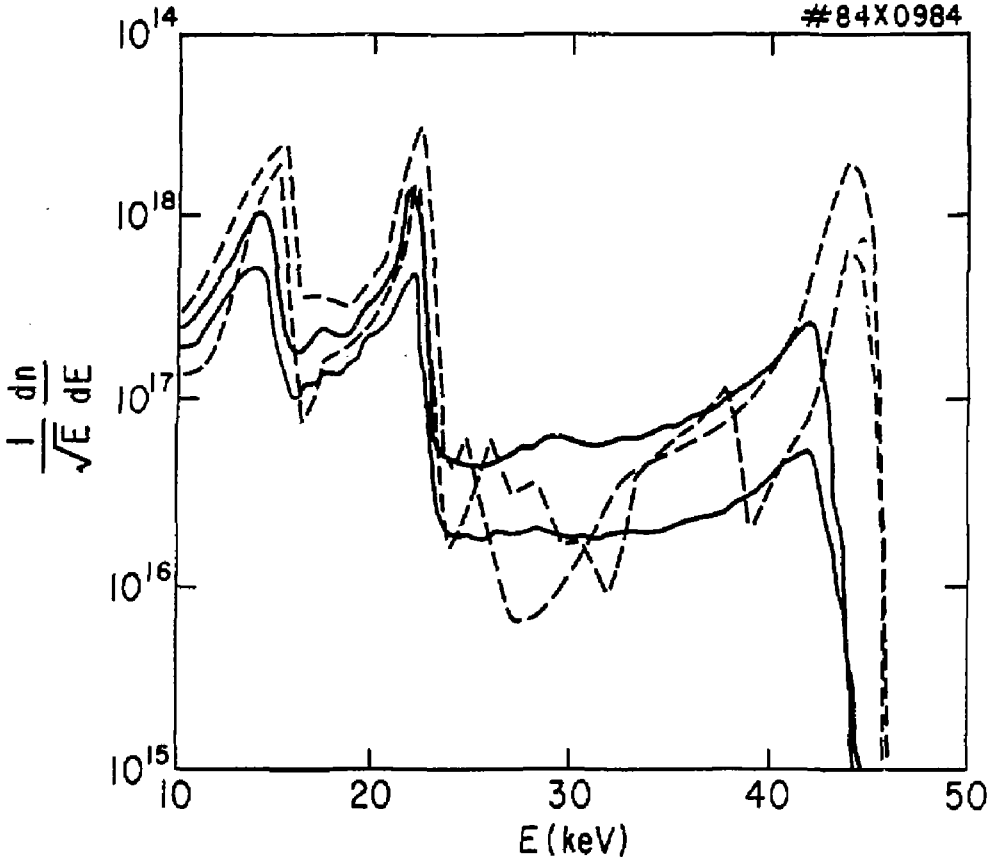
#84X0984
10^{14}
10^{18}
10^{17}
10^{16}
10^{15}
$\frac{1}{\sqrt{E}}\frac{dn}{dE}$
10
20
30
40
50
E (keV)

Fig. 17

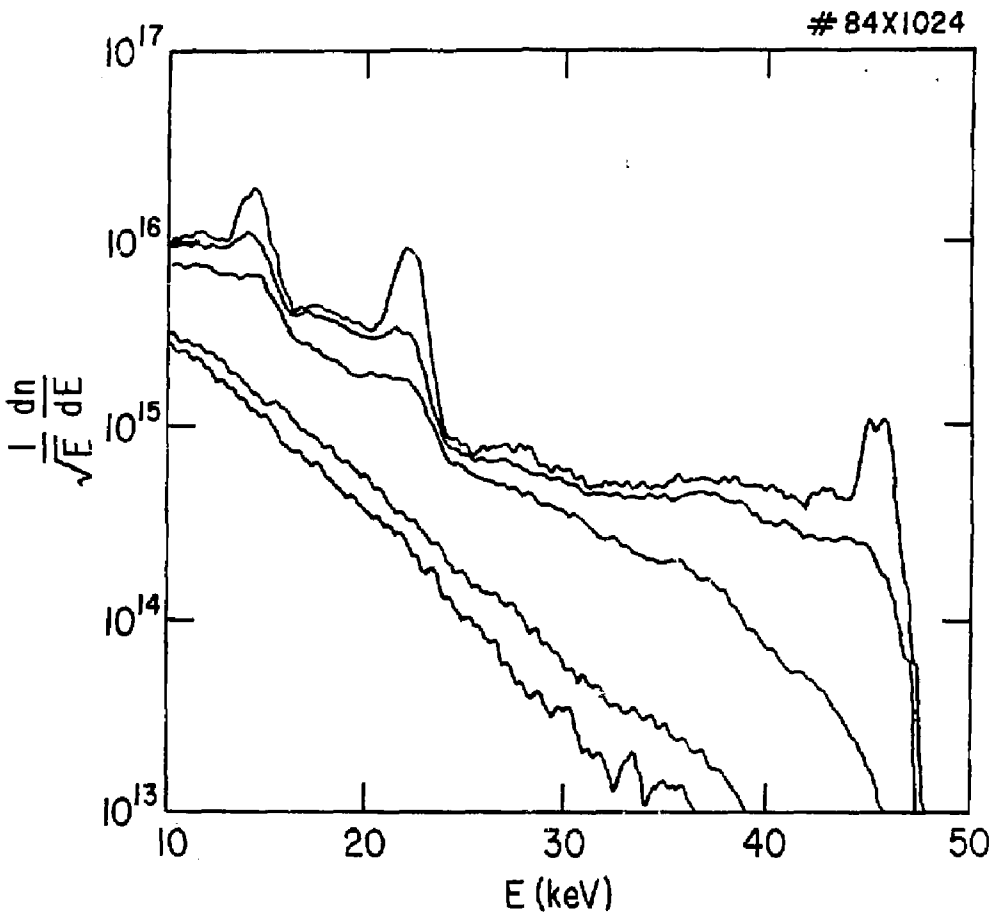
#84X1024
10^{17}
10^{16}
10^{15}
10^{14}
10^{13}
$\frac{1}{\sqrt{E}}\frac{dn}{dE}$
10
20
30
40
50
E (keV)

Fig. 18

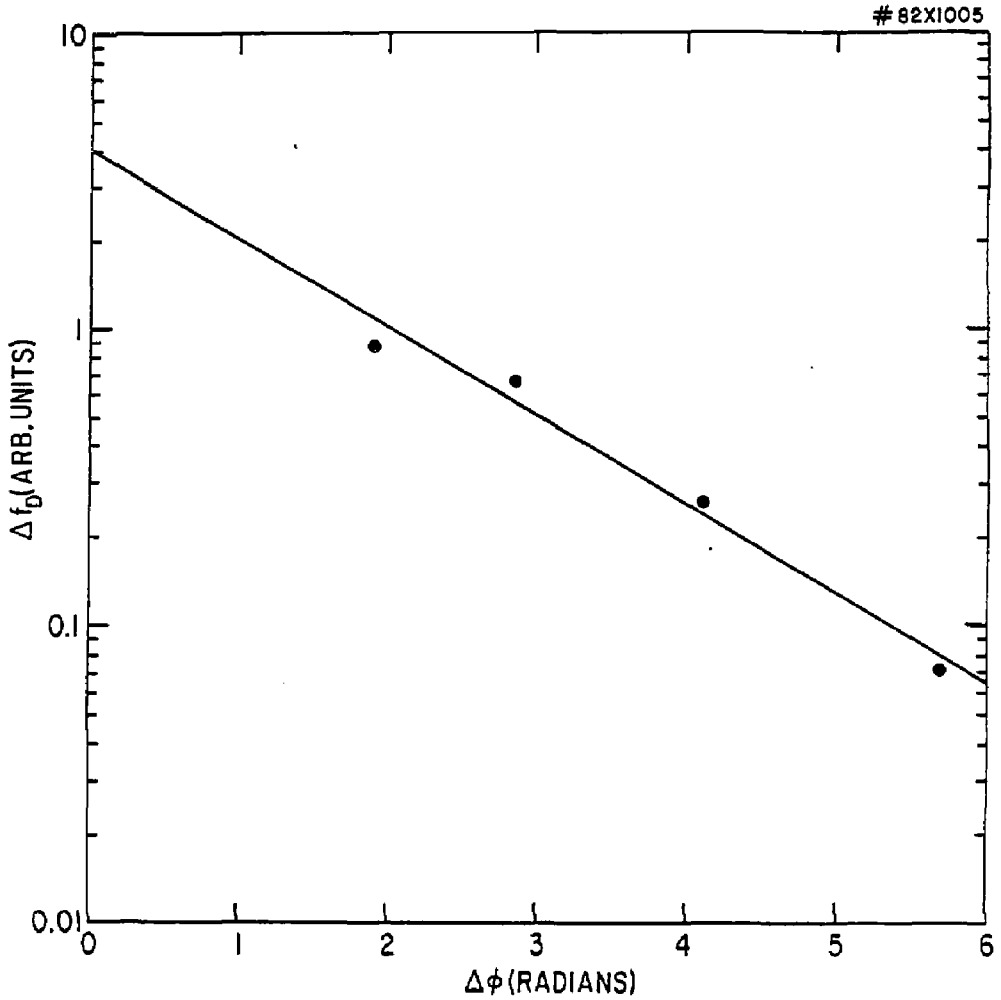
#82X1005
10
1
0.1
0.01
Δf_D(ARB. UNITS)
0
1
2
3
4
5
6
$\Delta\phi$(RADIANS)

Fig. 19

#84X0483

INITIAL 1/2 ORBITS WITH COUNTER INJECTION

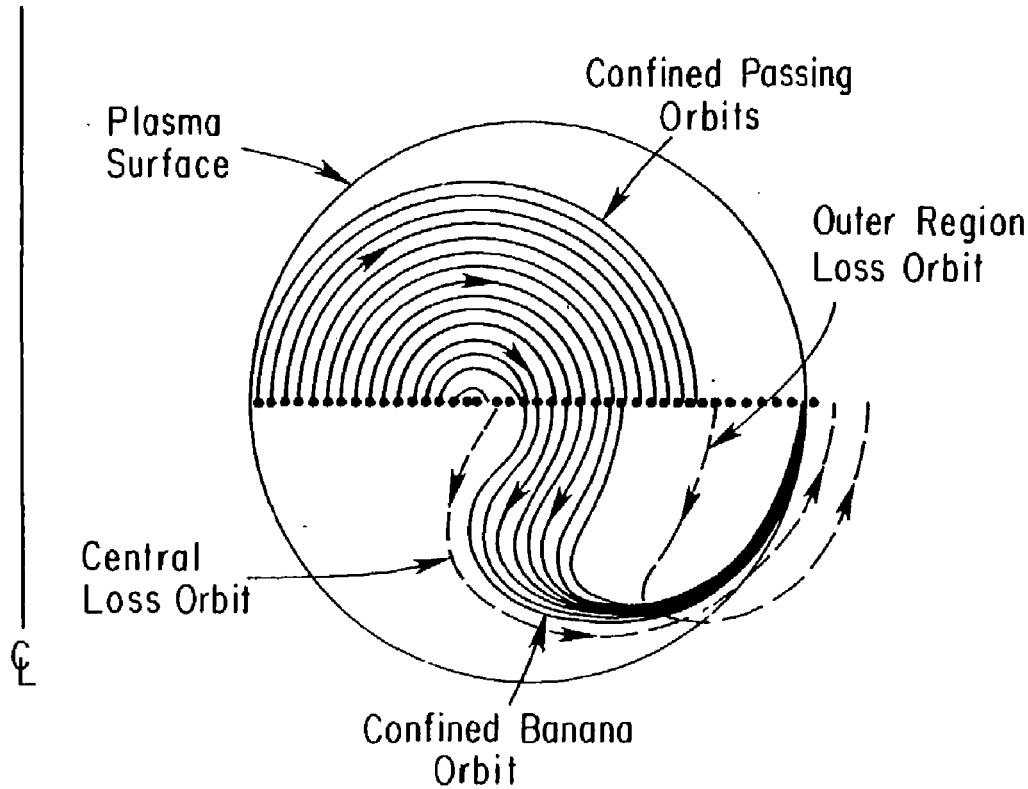

Fig. 20

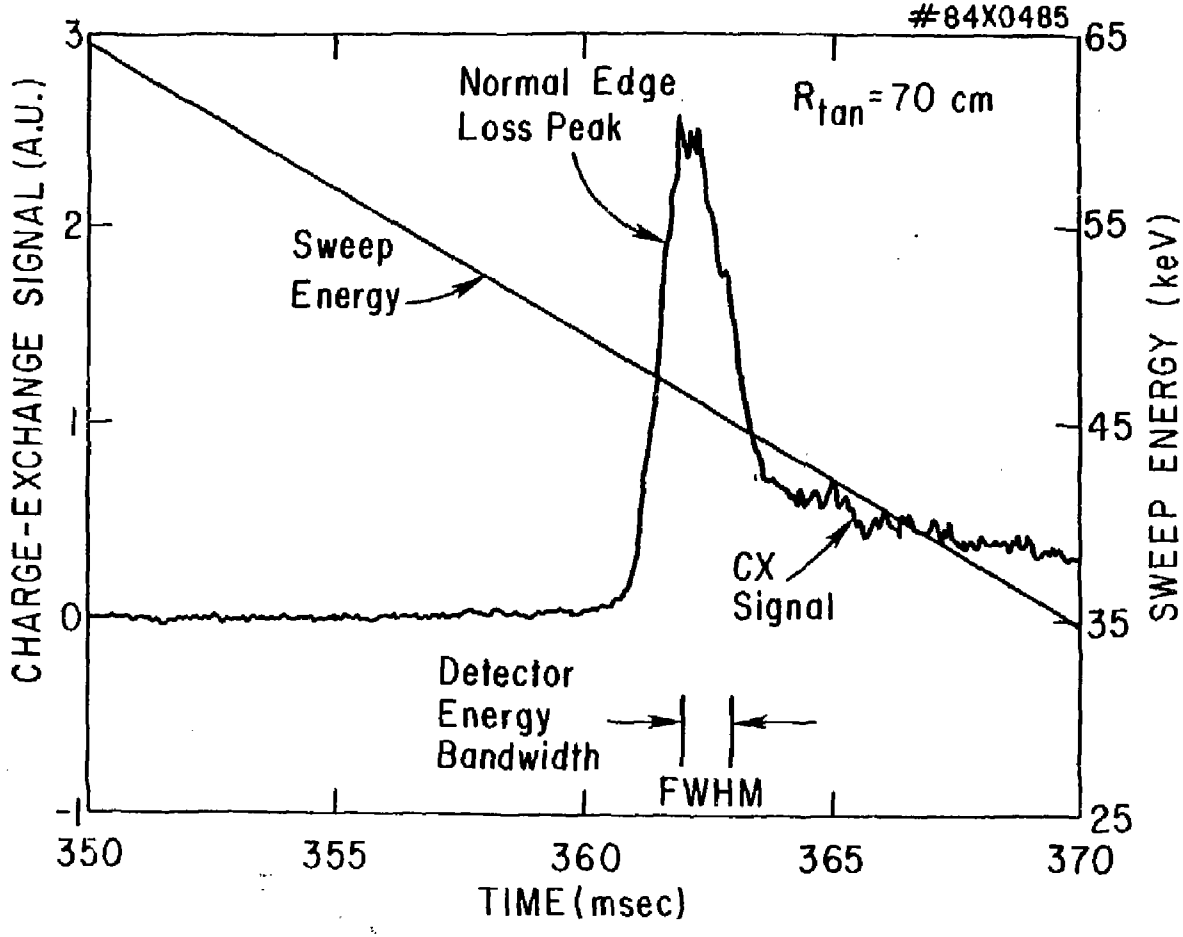
#84X0485
Normal Edge
Loss Peak
R_{tan}=70 cm
Sweep
Energy
CX
Signal
Detector
Energy
Bandwidth
FWHM
CHARGE-EXCHANGE SIGNAL (A.U.)
SWEEP ENERGY (keV)
TIME (msec)
3
2
1
0
-1
65
55
45
35
25
350
355
360
365
370

Fig. 21 (a)

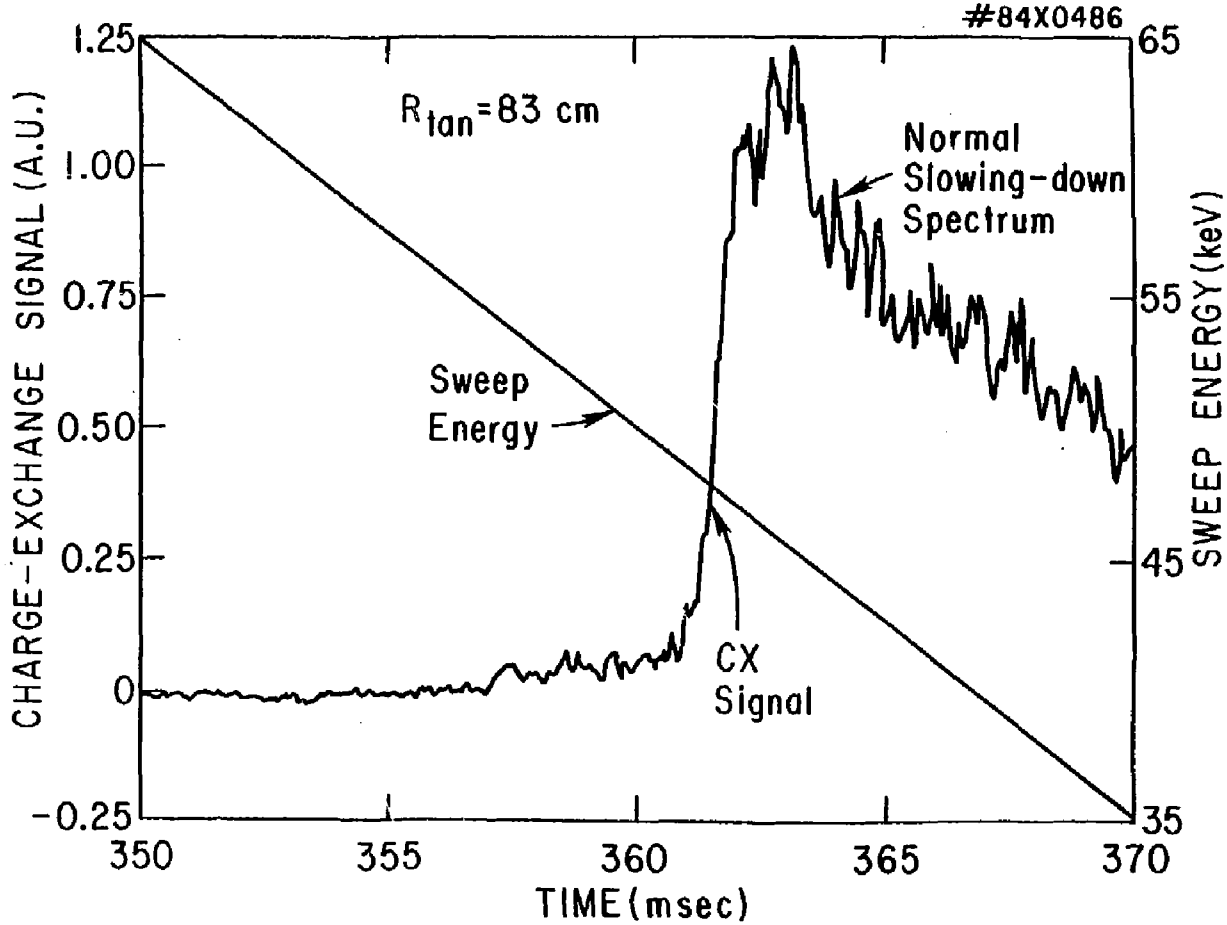
#84X0486
R_{tan}=83 cm
Normal
Slowing-down
Spectrum
Sweep
Energy
CX
Signal
CHARGE-EXCHANGE SIGNAL (A.U.)
SWEEP ENERGY (keV)
TIME (msec)
1.25
1.00
0.75
0.50
0.25
0
-0.25
65
55
45
35
350
355
360
365
370

Fig. 21 (b)

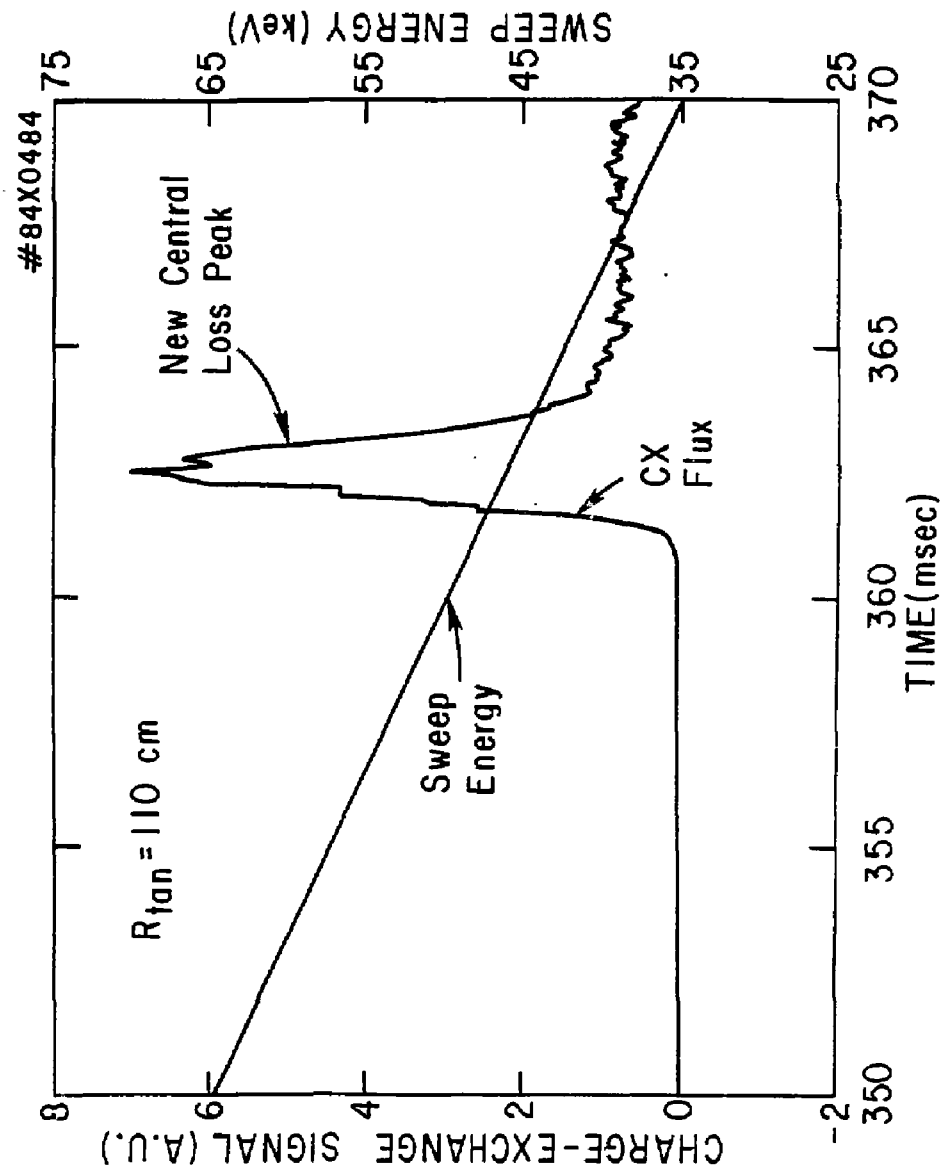
#84X0484
SWEEP ENERGY (keV)
75
65
55
45
35
25
New Central
Loss Peak
CX
Flux
Sweep
Energy
R_{tan} = 110 cm
CHARGE-EXCHANGE SIGNAL (A.U.)
8
6
4
2
0
-2
350
355
360
365
370
TIME(msec)

Fig. 21 (c)

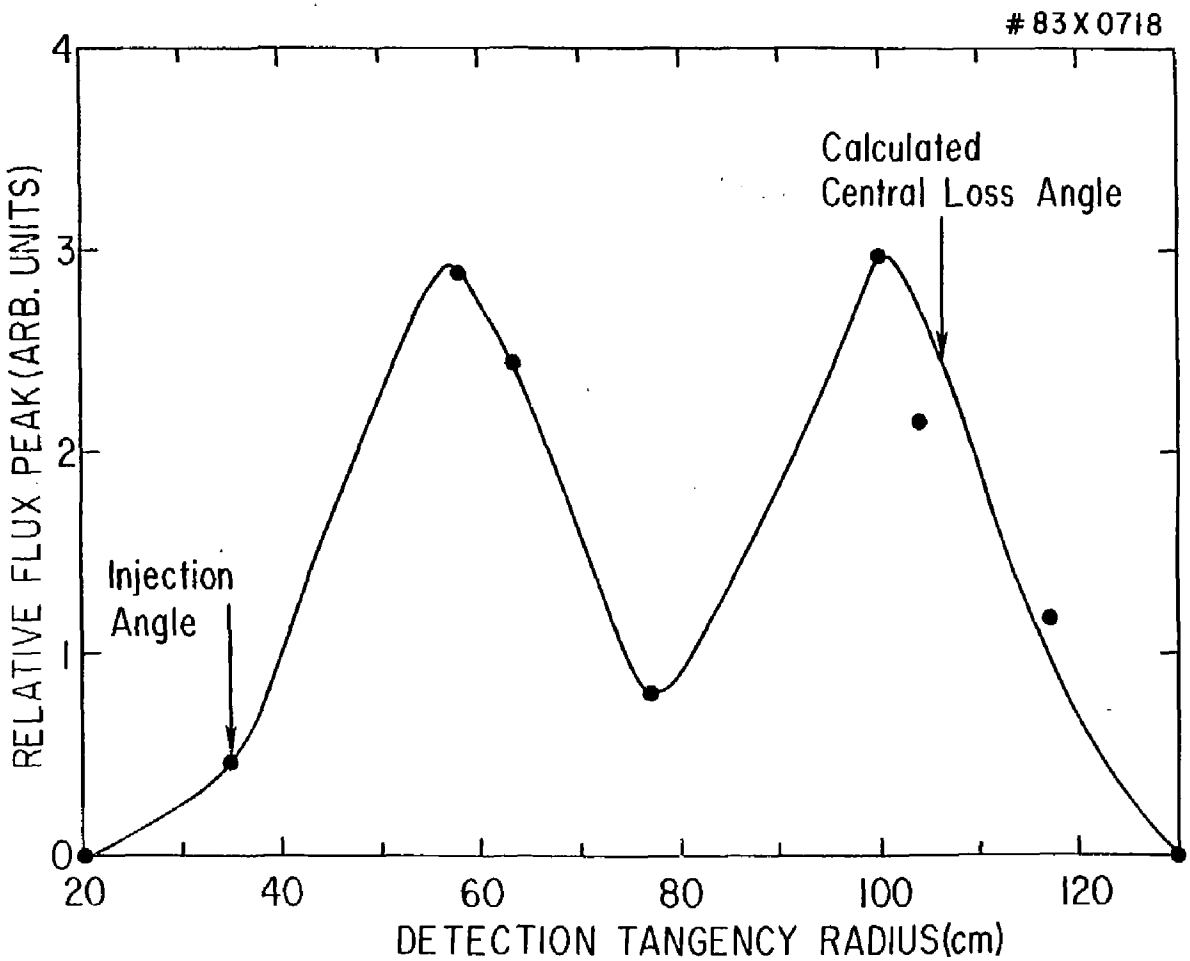
#83X0718
RELATIVE FLUX PEAK (ARB. UNITS)
0
1
2
3
4
Injection Angle
Calculated Central Loss Angle
20
40
60
80
100
120
DETECTION TANGENCY RADIUS(cm)

Fig. 22

EXTERNAL DISTRIBUTION IN ADDITION TO TIC UC-20

Plasma Res Lab, Austra Nat'l Univ, AUSTRALIA
Dr. Frank J. Paoloni, Univ of Wollongong, AUSTRALIA
Prof. I.R. Jones, Flinders Univ., AUSTRALIA
Prof. M.H. Brennan, Univ Sydney, AUSTRALIA
Prof. F. Cap, Inst Theo Phys, AUSTRIA
Prof. Frank Verheest, Inst theoretische, BELGIUM
Dr. D. Palumbo, Dg XII Fusion Prog, BELGIUM
Ecole Royale Militaire, Lab de Phys Plasmas, BELGIUM
Dr. P.H. Sakanaka, Univ Estadual, BRAZIL
Dr. C.R. Jones, Univ of Alberta, CANADA
Prof. J. Teichmann, Univ of Montreal, CANADA
Dr. H.M. Skarsgard, Univ of Saskatchewan, CANADA
Prof. S.R. Sreenivasan, University of Calgary, CANADA
Prof. Tudor W. Johnston, INRS-Energie, CANADA
Dr. Hannes Barnard, Univ British Columbia, CANADA
Dr. M.P. Bachynski, MPB Technologies, Inc., CANADA
Zhangwu Li, SW Inst Physics, CHINA
Library, Tsing Hua University, CHINA
Librarian, Institute of Physics, CHINA
Inst Plasma Phys, Academia Sinica, CHINA
Dr. Peter Lukac, Komenskeho Univ, CZECHOSLOVAKIA
The Librarian, Culham Laboratory, ENGLAND
Prof. Schatzman, Observatoire de Nice, FRANCE
J. Radet, CEN-BP6, FRANCE
AM Dupas Library, AM Dupas Library, FRANCE
Dr. Tom Mual, Academy Bibliographic, HONG KONG
Preprint Library, Cent Res Inst Phys, HUNGARY
Dr. S.K. Trehan, Panjab University, INDIA
Dr. Indra, Mohan Lal Das, Banaras Hindu Univ, INDIA
Dr. L.K. Chavda, South Gujarat Univ, INDIA
Dr. R.K. Chhajlani, Var Ruchi Marg, INDIA
P. Kaw, Physical Research Lab, INDIA
Dr. Phillip Rosenau, Israel Inst Tech, ISRAEL
Prof. S. Cuperman, Tel Aviv University, ISRAEL
Prof. G. Rostagni, Univ Di Padova, ITALY
Librarian, Int'l Ctr Theo Phys, ITALY
Miss Clelia De Palo, Assoc EURATOM-CNEN, ITALY
Biblioteca, del CNR EURATOM, ITALY
Dr. H. Yamato, Toshiba Res & Dev, JAPAN
Prof. M. Yoshikawa, JAERI, Tokai Res Est, JAPAN
Prof. T. Uchida, University of Tokyo, JAPAN
Research Info Center, Nagoya University, JAPAN
Prof. Kyoji Nishikawa, Univ of Hiroshima, JAPAN
Prof. Sigeru Mori, JAERI, JAPAN
Library, Kyoto University, JAPAN
Prof. Ichiro Kawakami, Nihon Univ, JAPAN
Prof. Satoshi Itoh, Kyushu University, JAPAN
Tech Info Division, Korea Atomic Energy, KOREA
Dr. R. England, Ciudad Universitaria, MEXICO
Bibliotheek, Fom-Inst Voor Plasma, NETHERLANDS
Prof. B.S. Liley, University of Waikato, NEW ZEALAND
Dr. Suresh C. Sharma, Univ of Calabar, NIGERIA
Prof. J.A.C. Cabral, Inst Superior Tech, PORTUGAL
Dr. Octavian Petrus, ALI CUZA University, ROMANIA
Prof. H.A. Hellberg, University of Natal, SO AFRICA
Dr. Johan de Villiers, Atomic Energy Bd, SO AFRICA
Fusion Div. Library, JEN, SPAIN
Prof. Hans Wilhelmson, Chalmers Univ Tech, SWEDEN
Dr. Lennart Stenflo, University of UMEA, SWEDEN
Library, Royal Inst Tech, SWEDEN
Dr. Erik T. Karlson, Uppsala Universitet, SWEDEN
Centre de Recherchesen, Ecole Polytech Fed, SWITZERLAND
Dr. W.L. Weiss, Nat'l Bur Stand, USA
Dr. W.M. Stacey, Georg Inst Tech, USA
Dr. S.T. Wu, Univ Alabama, USA
Prof. Norman L. Oleson, Univ S Florida, USA
Dr. Benjamin Ma, Iowa State Univ, USA
Prof. Magne Kristiansen, Texas Tech Univ, USA
Dr. Raymond Askew, Auburn Univ, USA
Dr. V.T. Tolok, Kharkov Phys Tech Ins, USSR
Dr. D.D. Ryutov, Siberian Acad Sci, USSR
Dr. G.A. Eliseev, Kurchatov Institute, USSR
Dr. V.A. Glukhikh, Inst Electro-Physical, USSR
Institute Gen. Physics, USSR
Prof. T.J. Boyd, Univ College N Wales, WALES
Dr. K. Schindler, Ruhr Universitat, W. GERMANY
Nuclear Res Estab, Julich Ltd, W. GERMANY
Librarian, Max-Planck Institut, W. GERMANY
Dr. H.J. Kaeppler, University Stuttgart, W. GERMANY
Bibliothek, Inst Plasmaforschung, W. GERMANY